A Review of Algorithms for Segmentation of Retinal Image Data Using Optical Coherence Tomography

Delia Cabrera DeBuc, PhD

Bascom Palmer Eye Institute, University of Miami Miller School of Medicine
United States of America

1. Introduction

In the context of biomedical imaging analysis and computer-assisted diagnosis, segmentation analysis is an intense field of research and development. The most difficult part of medical image analysis is the automated localization and delineation of structures of interest. Automated data evaluation is one way of enhancing the clinical utility of measurements. In particular, medical image segmentation extracts meaningful information and facilitate the display of this information in a clinically relevant way. A crucial role for automated information extraction in medical imaging usually involves the segmentation of regions of the image in order to quantify volumes and areas of interest of biological tissues for further diagnosis and localization of pathologies.

Optical coherence tomography (OCT) is a powerful imaging modality used to image various aspects of biological tissues, such as structural information, blood flow, elastic parameters, change of polarization states and molecular content (Huang et al., 1991). OCT uses the principle of low coherence interferometry to generate two or three dimensional imaging of biological samples by obtaining high-resolution cross-sectional backscattering profiles. A variety of successful algorithms for computer-aided diagnosis by means of OCT image analysis are presented in the literature, but robust use in clinical practice is still a major challenge for ongoing research in OCT image analysis. There are, therefore, efforts being made to improve clinical decision making based on automated analysis of OCT data. Particularly, in ophthalmology, efforts have been made to characterize clinically important features, such as damage to the fovea and optic nerve, automatically.

The transfer of image analysis models from algorithmic development into clinical application is currently the major bottleneck due to the complexity of the overall process. For example, the process to establish an application for OCT medical image analysis requires difficult and complex tasks that should considers the following actions: 1) to define the OCT image data structures representing relevant biomedical features and the algorithms determining a valid example for given image values, 2) to select meaningful values for all technical parameters of the image data structures and algorithms and, as a result, to configure such a method to operate on specific OCT clinical data, 3) to run the algorithm with the selected parameters to find the individual model instance that best explains the input image and 4) to validate the procedure to ensure a trustworthy result from an automated segmentation algorithm even if a gold standard is unavailable.

This chapter is intended to give a broad, but by no means complete, overview over common segmentation methods encountered in OCT retinal image processing. To do this, some algorithms that are representative for each class in some detail are described. In addition an understanding of the original derivation and motivation of each algorithm is provided, instead of merely stating how each method functions. This is of high importance in order to get an idea where and under what circumstances a method can function and when one can expect an algorithm to fail. To briefly motivate why one should consider different segmentation algorithms, consider the example of a 2D OCT image in Fig. 1. Simple thresholding can be used to mark the locations of the inner and outer boundaries of the retina in this OCT image. But some boundary sections are not properly identified due to poor contrast or low resolution, making it impossible to identify the exact extent of the retina in this image (see Fig.1A). Since these boundaries are found by a threshold procedure, their estimated locations could be sensitive to relative differences in reflectance between the outer and deeper retinal structures. By choosing a different segmentation algorithm (see Fig. 1B), identification of the retinal boundaries can be improved (Cabrera Fernández et al., 2005b). All segmentation methods that have been proposed in the literature aim at improving retinal image segmentation in this or other aspects. The causes for problems such as the ones in Fig. 1 can by manifold, many times being inherent to the respective image acquisition method itself.
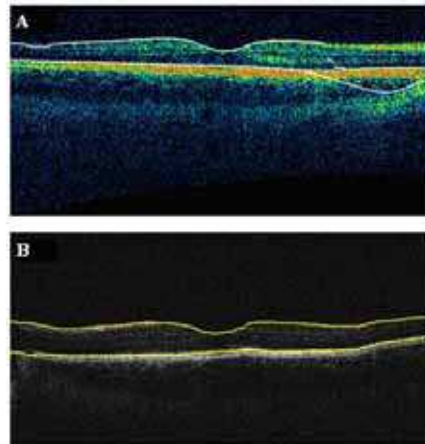

Fig. 1. Segmentation results showing the performance of the Stratus OCT custom built-in algorithm compared to the results using a custom algorithm. A) Macular scan obtained from a healthy eye. Note the misidentification of the outer boundary of the retina outlined in white. B) Results obtained for the same eye using a custom algorithm. Note that the custom algorithm was able to correctly detect the outer boundary of the retina.

The chapter is organized as follows. The next section continues with an outline of current retinal imaging modalities. Section 3 explains the physical principles and technical details of how OCT works. The interpretation of the OCT image along with the current and future technology development of OCT systems is also presented in this section. Section 4 provides the necessary background about medical image segmentation approaches. A review of algorithms for segmentation of retinal image data using OCT is presented in Section 5. All

published (within the author's awareness) papers related to retinal image segmentation are gathered into this single compilation. Section 6 offers some concluding remarks.

2. Current retinal imaging modalities

Millions of people worldwide live with retinal disease and the accompanying threat of severe vision loss or blindness. During the last few years, the retinal research field has undergone a dramatic change in terms of diagnostic tools and therapies that have resulted in substantial benefits for patients suffering from retinal disease. Traditionally the retina has been observed either directly via an ophthalmoscope or similar optical devices such as the fundus camera. The field of ophthalmology was revolutionized in 1851 with the invention of the ophthalmoscope by Hermann von Helmholtz (von Helmholtz, 1851) as for the first time detailed examinations of the interior of the eye could be made in living patients. The ophthalmoscope and later the fundus camera remained the primary methods of ocular examination into the 1960's, and they are standard tools still effective and in use today, although they are not without limitations, and both require trained users to operate and make diagnoses.

With advances in medical technology, more powerful techniques were introduced. In 1961 fluorescein angiography was developed by Novotny and Alvis, a procedure in which sodium fluorescein is injected into a vein, and under filtered light the sodium fluorescein within the blood fluoresces, glowing brightly and providing easily observed patterns of blood flow within the eye (Novotny & Alvis, 1961). This allows the arteries, capillaries and veins to be easily identified and photographed, and from this, large amounts of information concerning the health or otherwise of the circulatory system can be determined.

During the 1990's the indocyanine green dye angiography technique was developed; similarly to the flourescein angiography a dye is injected into the bloodstream, however the indocyanine green dye glows in the infra-red section of the spectrum. The indocyanine green dye approach only came into widespread use when digital cameras sensitive into the infra-red became commonly available, and it complements fluorescein angiography by highlighting different aspects of the vasculature of the eye. In particular it enhances the structure of the choroid, which is the layer of blood vessels beneath the retina. These two techniques can be used together to gain a more thorough understanding of the structure and pathologies affecting an eye. They can illustrate patterns of blood flow, haemorraging and obstructions within the vascular system, but, like the ophthalmoscope, both require trained medical staff to perform the procedure, and a clinical environment where the images can be taken and analyzed. In addition to these methods for observing the vasculature of the eye there are a range of other, more advanced, methods of mapping structures and changes within the eye, including ultrasound, OCT and laser-based blood flowmeters in development and in use. All of these can be used to scan the eye and make observations and diagnoses on the eye and circulatory system. Specifically, the introduction of OCT imaging in daily routine have resulted in some of the central changes to retinal disease understanding and management. Figure 2 shows the operational range of the OCT technology compared to standard imaging.

OCT is a rapidly emerging medical imaging technology that has applications in many clinical specialties. OCT uses retroreflected light to provide micron-resolution, cross-sectional scans of biological tissues (Hee et al., 1995; Huang et al., 1991; Izatt et al., 1994a).
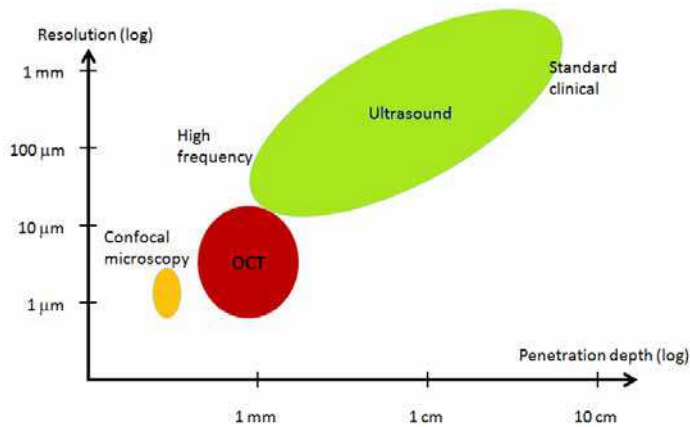
Fig. 2. OCT vs. standard imaging.

The first micron-resolution OCT system for imaging human retina *in vivo* was introduced in 1991 (Huang et al., 1991). In ophthalmology; OCT is a powerful medical imaging technology because it enables visualization of the cross- sectional structure of the retina and anterior eye with higher resolutions than any other non-invasive imaging modality (Huang et al., 1991). The depth resolution of OCT is extremely fine, typically on the order of 0.01mm or 0.4 thousandth of an inch. An OCT image represents a cross-sectional, micron scale picture of the optical reflectance properties of the tissue (Huang et al., 1991). This image can either be used to qualitatively assess tissue features and pathologies or to objectively make quantitative measurements.

While this is just a brief introduction to some of the diagnostic tools available to obtain retinal images, to draw diagnoses from these images requires specialist training, and to adequately extract and track the retinal damage from the images often takes extensive image processing and analysis. Once automatic image analysis is possible, those at risk of numerous diseases and problems of the retinal tissue can be rapidly identified and referred for further treatment. The development of this methodology would also allow automated tracking of the progress of such health problems as diabetic retinopathy, and track changes in the eyes as the subject ages. This would have numerous health benefits, including providing an early prediction of retinal diseases.

3. Optical coherence tomography background

The clinical potential of OCT technology in ophthalmology was originally recognized in the early 1990s. OCT is an extension of optical coherence domain reflectometry to imaging in two or three dimensions (Brezinski et al., 1996). This imaging technique generates a cross-sectional image by recording axial reflectance profiles while the transverse position of the optical beam on the sample is scanned. Thus, the longitudinal location of tissue structures are determined by measuring the time-of-flight delays of light backscattered from these structures. The optical delays are measured by low coherence interferometry. Light reflected from deeper layers has a longer propagation delay than light reflected from more superficial layers.

Conventional or time domain OCT (TDOCT) is based on the principle of low coherence interferometry which is a powerful tool to section a transparent object. Low coherence

means that the system employs a wide range of wavelengths. The most straightforward and currently the most common interferometer for OCT is a simple Michelson interferometer (see Fig 3) (Michelson & Morley, 1887). A low-coherence source illuminates the interferometer. The light is split by a 50/50 beamsplitter into a sample and a reference path. Light retroreflected from the reference and the sample is recombined at the beamsplitter and half is collected by a photodetector in the detection arm of the interferometer. Half of the light is returned towards the source, where it is lost. In addition, the reference arm light is typically attenuated by orders of magnitude in order to improve signal to noise ratio.
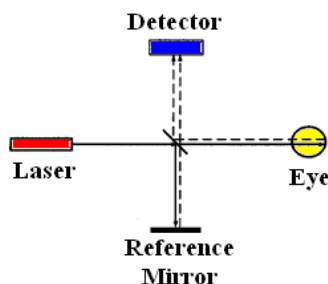

Fig. 3. Schematic drawing of the principle of OCT emphasizing how it is essentially a Michelson intereferometer. The outgoing light paths are solid lines, while reflected light is drawn as dashes lines.

The axial resolution of an OCT image depends on the coherence length which is a fundamental property of the light source, whereas transverse resolution for OCT imaging is determined by focused spot size, as in microscopy. By rapidly varying the reference arm mirror and synchronously recording the magnitude of the resulting interference signal, a single axial profile or A-scan is obtained which is a graph of the optical reflectivity versus distance in the eye. A sequence of such A-scans is obtained by scanning the probe beam across the entire retina which forms a B-scan tomogram. As a result, a cross-sectional view of the structure similar to a histology section is obtained.

OCT can be used for retinal imaging and anterior segment imaging. The OCT for ophthalmic examination is similar to a slit lamp for anterior segment imaging and a fundus camera for retinal imaging. The instrumentation includes a video display for operator viewing of the anterior segment or fundus while obtaining the OCT images and a simultaneous computer display of the tomograms. Images are stored via computer for the diagnostic record (Puliafito, 1996).

3.1 Interpreting OCT images

The OCT signal from a particular tissue layer is a combination of its reflectivity and the absorption and scattering properties of the overlying tissue layers. Strong reflections occur at the boundaries between two materials of different refractive indices and from a tissue that has a high scattering coefficient along with a disposition to scatter light in the perfectly backward direction (Huang et al., 1991; Puliafito, 1996). Thus, an OCT image is a map of the reflectivity of the sample. In most tissues, main sources of reflection are collagen fiber bundles, cell walls, and cell nuclei. Dark areas on the image represent homogeneous material with low reflectivity, such as air or clear fluids. The imaging light is attenuated in the sample, so there is an

exponential decrease in the intensity of the image with depth. Blood attenuates the signal faster than collagenous tissues, fat and fluids attenuate the signal the least.

In OCT images, the signal strength is represented in false color. High backscatter appears red-orange and low backscatter appears blue-black (see Fig. 4). Thus, tissues with different reflectivity are displayed in different colors. It is important to note that OCT image contrast arises from intrinsic differences in tissue optical properties. Thus, coloring of different structures represents different optical properties in false color image and it is not necessarily different tissue pathology (see Fig. 4). The exact relationship between the histology of the tissue and the OCT map is still under investigation. Relative high reflectivity layers correspond to areas of horizontal retinal elements such as the nerve fiber layer at the retinal surface or deeper plexiform layers and a single layer of retinal pigment epithelium (RPE) and choroid. Relative low reflectivity layers correspond to the nuclear layers and a single layer of photoreceptor inner and outer segments. Warm colors (red to white) represent areas of relative high reflectivity, while cold colors (blue to black) represent areas of relative low reflectivity.

In the retina, the vitreoretinal interface is demarcated by the reflections from the surface of the retina. The retinal pigment epithelium (RPE) and choriocapillaris layer (ChCap) is visualized as a highly reflective red layer and represents the posterior boundary of the retina. Below the choriocapillaris weakly scattered light returns from the choroid and sclera because of attenuation of the signal after passing through the neurosensory retina, RPE, and ChCap. The outer segments of the rods and cones appear as a dark layer of minimal reflectivity anterior to the RPE and ChCap. The intermediate layers of the retina exhibit moderate backscattering (see Fig. 4). The fovea appears as a characteristic thinning of the retina. The lateral displacement of the retina anterior to the photoreceptors is evident (see Fig. 4).
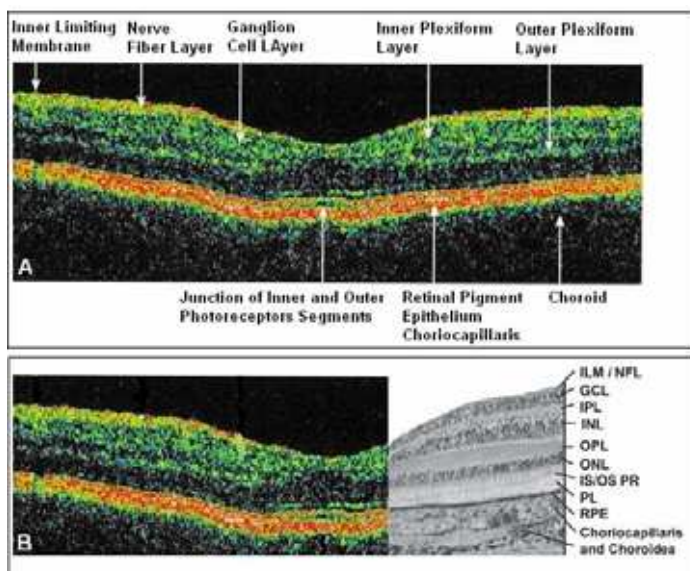

Fig. 4. OCT image of the normal human macula. (A) Stratus OCT image showing the various cellular layers of the retina. (B) Comparison of the OCT image (same as shown in A) to a histologic micrograph of the normal human macula.

3.2 Quantitative measurements of retinal morphology

OCT can aid in identifying, monitoring and quantitatively assessing various posterior segment conditions including macular edema, age-and-non-age related macular degeneration, full and partial-thickness macular hole, epiretinal membrane, intaretinal exudate, idiopathic central serous chorioretinopathy, RPE detachment, detachment of the neurosensory retina, and macular lesions associated with optic nerve head pits or glaucoma Figure 5 shows exemplary images of two of the above cited pathological cases obtained with a RTVue FD-OCT system (Optovue Inc., Freemonth, CA).
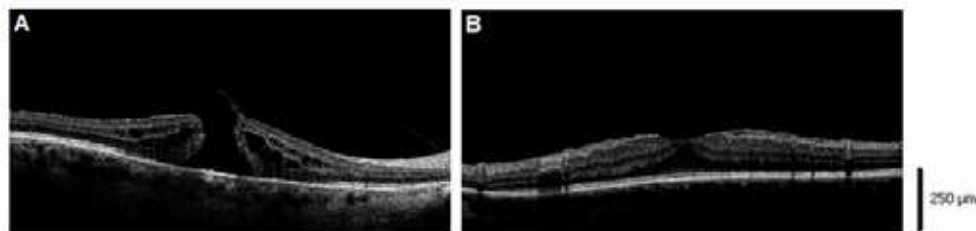

Fig. 5. OCT images showing two OCT B-scans (6 mm length) from pathological retinas. A) Macular hole, B) Epiretinal membrane.

As a matter of fact, OCT can demonstrate the presence of edema where it is not seen on biomicroscopy or angiographically. A very important feature of the OCT system is that it provides information on the retinal structures. For example, the location of fluid accumulation in relation to the different retinal layers may be determined and the response to treatment without the need to perform invasive studies such as fluorescein angiography may be objectively monitored. At the same time it may be possible to explain why some patients respond to treatment while others do not. OCT has significant potential both as a diagnostic tool and particularly as a way to monitor objectively subtle retinal changes induced by therapeutic interventions. Thus, OCT may become a valuable tool in determining the minimum maintenance dose of a certain drug in the treatment of retinal diseases, and may demonstrate retinal changes that explain the recovery in some patients without angiographically demonstrable improvement and lack of recovery in others.

In the clinical routine, measurement of retinal thickness by the OCT software depends on the identification of the internal limiting membrane and the hyper-reflective band believed to correspond to the retinal pigment epithelium – choriocapillaris interface (or, more precisely, the photoreceptor inner-outer segment border in the case of third generation OCTs). The OCT software algorithms calculates the distance between these 2 boundaries across all of the sampled points and interpolates the retinal thickness in the unsampled areas between these lines. However, once the various layers can be identified and correlated with the histological structure of the retina, it may seem relevant to measure not only the entire thickness of the retina, but the thickness of the various cellular layers. Moreover, measuring the reflectance of the various retinal layers on OCT images may also be of interest. Drexler et al. have shown in *in vitro* and *in vivo* (Bizheva et al., 2006; Hermann et al., 2006) studies that physiological processes of the retina lead to optical density changes that can be observed by a special M-mode OCT imaging, known as optophysiology. Thus, it also seems rational that quantitative analysis of reflectance changes may provide clinically relevant information in retinal patophysiology.

3.3 Recent developments in OCT technology

The emergence of ultrabroad bandwidth femtosecond laser technology has allowed the development of an ultra-high resolution OCT, which has been demonstrated to achieve axial resolutions of 3 μm during *in vivo* imaging of the human retina, which is two orders of magnitude higher than what can be achieved by conventional ultrasound imaging. Figure 6 shows the ultrahigh resolution OCT cross section of a normal human macula showing all of the major layers and internal structures of the retina. The ultrahigh resolution OCT will in effect be a microscope capable of revealing certain histopathological aspects of macular disease in the living eye.

As it was previously explained, in the conventional or time domain OCT (TDOCT) system the length of the reference arm in an interferometer is rapidly scanned over a distance corresponding to the imaging depth range. The mechanism of scanning largely limits the acquisition speed and makes real-time imaging impossible. In recent years a new model OCT based on Fourier domain interferometry has emerged, and it has been called spectral domain OCT (SDOCT) or Fourier domain OCT (FDOCT) (Fercher et al., 1995; Fercher et al., 2003; Hausler & Lindner, 1998). SDOCT can avoid scanning of the reference, thus it can reach very high acquisition speed. As a matter of fact, in time domain OCT the location of scatters in the sample is observed by generation of interferometric fringes at the detector as the reference reflector position is axially translated. In contrast, Fourier domain OCT required the reference arm to be held fixed, and the optical path length difference between sample and reference reflections is encoded by the frequency of the interferometric fringes as a function of the source spectrum. Two configurations have prevailed in Fourier domain systems: spectral domain (SD) OCT uses a grating to spatially disperse the spectrum across an array-type detector, and in swept source (SS) OCT a narrow band laser is swept across a broad spectrum, encoding the spectrum as a function of time. SDOCT offers a significant sensitivity advantage over TDOCT (Choma et al., 2003; de Boer et al., 2003, Leitgeb et al., 2003; Mitsui, 1999).
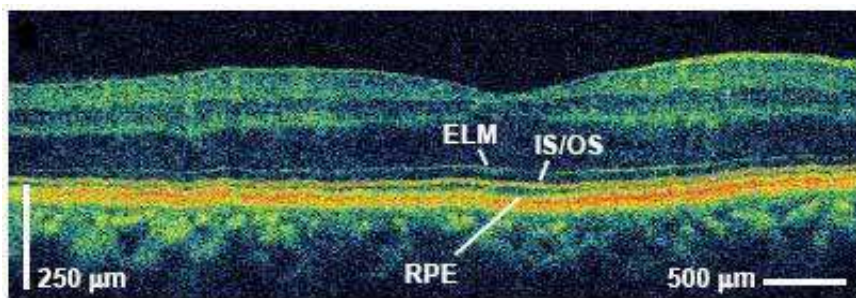

Fig. 6. Ultrahigh resolution OCT cross section of a normal human macula with 3 microns resolution (Courtesy "James Fujimoto," (Fujimoto et al., 2003)).

New technology has also been developed to improve resolution in the transverse dimension. In the current commercial application of OCT, the transverse resolution is limited by the intrinsic ocular aberrations of the eye. The transverse resolution can be significantly improved by correcting the aberrations across a large pupil using adaptive optics (AO). A high axial (3 μm) and improved transverse (5–10 μm) resolution AO-OCT system was demonstrated for the first time in *in vivo* retinal imaging (Hermann et al., 2004).

The instrument uses a wavefront sensor that measures the aberrations in patient's eyes and then adjusts the surface of an adaptive mirror to correct the visual flaws. An improvement of the transverse resolution of two to three times, compared with ultrahigh resolution OCT systems used so far, was obtained by using adaptive optics A significant signal-to-noise ratio improvement of up to 9 dB in corrected compared with uncorrected OCT tomograms was also achieved. Zawadzki et al. also demonstrated the ability to image microscopic blood vessels and the cone photoreceptor mosaic using an AO-OCT instrument with high 3D resolution(4x4x6 μm) (Zawadzki et al., 2005). AO-OCT is currently the only option for studying living retinal tissue at the cellular level and clinical trials of the instrument are still being performed.

Another limitation of OCT technology has been the difficulty in accurately localizing the cross-sectional images and correlating them with a conventional en face view of the fundus. One way to localize and visually interpret the images would be to integrate a scanning laser ophthalmoscope (SLO) into the OCT, thereby mapping OCT pixels to the conventional en face view of the SLO. This rationale was used by Ophthalmic Technologies Inc (Toronto, Canada) to develop the Spectral OCT-SLO in 2004 (Podoleanu et al., 2004). The system simultaneously produces SLO and OCT images that are created through the same optical path, and therefore correspond pixel to pixel. OCT-SLO, offers multiple views from a single scan with perfect registration of images. OCT-SLO imaging offers very accurate localisation of pathology with enhancement of the vitreoretinal interface. Its ability to align serial topographies and to fuse other modalities, with real-time, ultrahigh resolution capability and multi-planar anterior segment imaging should make it an invaluable addition to the diagnostic arsenal of the vitreoretinal surgeon.

A number of other instruments have also been built based on variations of the basic OCT system. For instance, polarization-sensitive optical coherence tomography (PS-OCT) uses polarization-altering optics in the arms of the interferometer to determine the sample birefringence from the magnitude of the back-reflected light (de Boer et al., 1997; de Boer et al., 2003). This instrument can be used to assess effects such as retinal nerve fiber layer thickness (Cense et al., 2002), early osteoarthritic changes in cartilage (Hermann et al., 1999) or burn depth in thermally damaged tissue (de Boer et al., 1998). Optical coherence microscopy (OCM) is a hybrid instrument that uses a system of high numerical aperture to achieve resolutions comparable to confocal microscopy but with increased depth of penetration (Izatt et al., 1994b). This instrument has been applied to gastrointestinal tissues and promises to enable endoscopically based cellular imaging (Izatt et al., 1996; Aguirre et al., 2003). Doppler optical coherence tomography (Doppler OCT) is an augmentation capable of simultaneous blood flow mapping and spatially resolved imaging (Chen et al., 1997; Izatt et al., 1997; Westphal et al., 2002; Wong et al., 2002; Yazdanfar et al., 2003; Zhao et al., 2000; Ding et al., 2002; Ren et al., 2002). Doppler flow measurements can be performed by measuring the Doppler shift of light scattered from blood. Doppler OCT has been used to explore the human retinal flow dynamics (Yazdanfar et al., 2003); and it is a promising imaging technology for quantitatively assessing capillarity density and angiogenesis (Fujimoto et al., 2003).

Functional OCT imaging is another emerging modality that facilitates the assessment of functional or biochemical properties of the investigated tissue. Spectroscopic OCT imaging using broadband light sources enables the spectrum of the backscattered light from each pixel to be measured (Morgner et al., 2000). This extension of OCT is closely related to classical Fourier transform infrared spectroscopy and has the advantage that the

spectroscopic information can be acquired at multiple wavelengths across the available bandwidth of the light source in a single measurement (Boppart et al., 1999). The potential of Spectroscopic OCT in developmental and cellular biology is really promising.

As it can be seen, a wide range of OCT imaging platforms with rapidly emerging applications spanning a range of fields has been developed. The rapid advances in OCT imaging are likely to alter the practice of ophthalmology dramatically in the next several years. Increased resolution and imaging speeds, wavefront correction, improved multiple functionality of the OCT systems; and the possibility of quantitative 3D modeling are just a few of the features to look for in the future. Further advances may transform the OCT from an ancillary procedure to a common and necessary "optical biopsy". Indeed, future ophthalmologists will use the next generation of OCT devices as a broad based tool for comprehensive ophthalmic examinations; and may even diagnose macular disorders exclusively by digital imaging, without a funduscopic examination.

4. Medical image segmentation approaches

Imaging operations may be broadly classified according to four categories: preprocessing, visualization, manipulation and analysis. Segmentation is a common used operation in preprocessing approaches and an essential operation for most visualization, manipulation and analysis tasks in image processing (see Fig. 7). Segmentation is, therefore, the most critical among all imaging procedures, and also the most challenging.

Segmentation purpose is to identify and delineate objects. Here, an object refers to any physical object such as an anatomical organ or a pathological entity such as a tumor or cyst (see Fig. 8). Segmentation is defined as the partitioning of an image into non-overlapping, component regions which are homogeneous with respect to some characteristic such as intensity or texture (Haralick et al., 1985; Gonzalez & Woods, 1992; Pal & Pal, 1993). Typically, image segmentation consist of two related tasks: recognition and delineation. Recognition consists of determining approximately the objects' location in the image. For example, in Figure 9, this task involves determining the location of the RNFL, GCL, IPL, etc. This does not involve the precise specification of the region occupied by the object. Delineation involves determining the objects' precise spatial extent and composition including gradation of intensities. In Figure 9 again, if retinal tissue is the object structure of interest, then delineation consists of the spatial extent of the RNFL and GCL separately, and for each element (i.e. pixels for 2D and voxels for 3D) in each object, specifying a characteristic value of the object (for example, RNFL thickness or volume). Once the objects are defined separately, the RNFL and GCL can be individually visualized, manipulated and analyzed. While automatic and human-assisted are the only two approaches for recognition tasks, numerous methods are available for delineation. Approaches to delineation can be classified as: 1) boundary-based and 2) region-based (Kim & Hori, 2000).

Numerous approaches regarding image segmentation techniques are available in the literature. Some of these techniques use only the gray level histogram, some use spatial details while others use fuzzy set theoretic approaches. Most of these techniques are not suitable for noisy environments. In particular, segmentation approaches can be classified according to the methodology used in the segmentation strategy (see Fig. 10):

1. *Classical segmentation methods*: These approaches classically partition an image into non-overlapping segments which are homogeneous with respect to some characteristic such as intensity or texture (Haralick et al., 1985; Gonzalez & Woods, 1992; Pal & Pal, 1993).
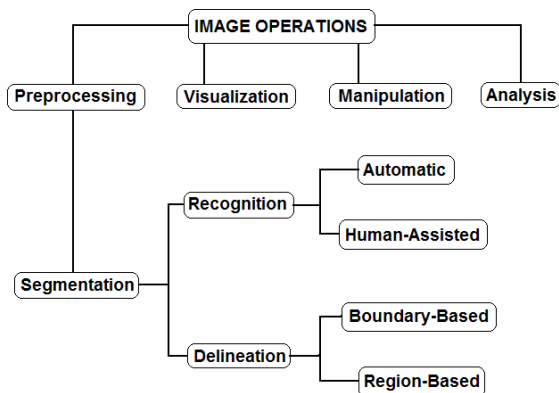
Fig. 7. Classification of image operations.

Fig. 8. OCT image segmentation results showing isolated retinal features of interest. A) OCT B-scan showing multiple lesions in the central retinal area of a patient with age related macular degeneration. Macular cysts and the subretinal fluid area were segmented using a deformable model (Cabrera Fernández et al., 2005a). B) Segmentation result showing the intraretinal layers outlined on an OCT B-scan section obtained from a healthy subject .

2. *Pixel classification methods*: These methods basically do not require the constraint that regions be connected. Thresholding, classifier, clustering, and Markov random field (MRF) approaches can be considered pixel classification methods. Thresholding is the most intuitive approach to segmentation (Sahoo et al., 1988). Specifically, algorithms based on threshold create a partitioning of the image based on quantifiable features, like image intensity or gradient magnitude. These algorithms map and cluster pixels in a feature space called a histogram. Thresholds are chosen at valleys between pixel clusters so that each pair represents a region of similar pixels in the image. The segmentation is then achieved by searching for pixels that satisfy the rules defined by the thresholds. Thresholds in these algorithms can be selected manually according to a priori knowledge or automatically through image information. Thresholding algorithms can be divided into edge-based ones (e.g. Canny edge detector and Laplacian edge detector), region-based ones (e.g. region growing algorithms) and hybrid ones (e.g. watershed algorithms). Edge-based algorithms attempt to find edge pixels while eliminate the noise influence. Thresholds in the edge-based algorithms are related with the edge information. Region-based algorithms exploit the fact that pixels

inside a structure tend to have similar intensities. Region growing algorithms, once initial seeds are selected, search for the neighboring pixels whose intensities are inside the intervals defined by the thresholds and then merge them to expand the regions. Hybrid algorithms fuse region information with a boundary detector to complete the segmentation. Typical hybrid algorithms are the level set method with regularizers and the watershed algorithm. Particularly, the watershed algorithms (Yezi et al., 1999) combine the image intensity with the gradient information. In addition, the methodology of using MRF based methods to the problem of segmentation has received a great deal of attention in the past decade (Tamás et al., 2000). MRF modeling itself is not a segmentation method but a statistical model which can be used within segmentation methods. As shown in Fig. 10, MRF is a region-based approach. MRF models spatial interactions between neighboring or nearby pixels. Hence, the classification of a particular pixel is based, not only on the intensity of that pixel, but
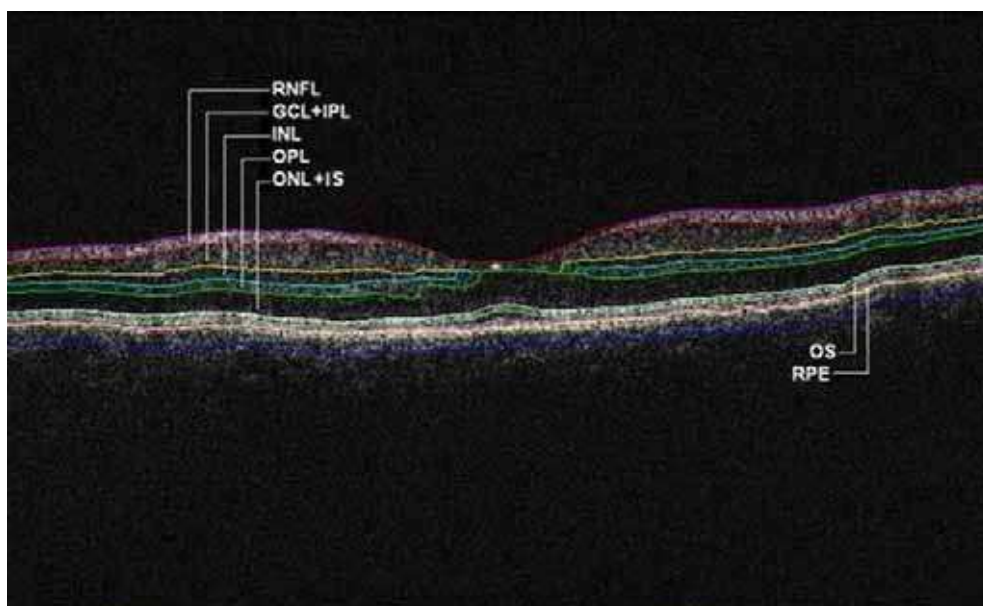

Fig. 9. Segmentation results for an OCT B-scan obtained from a healthy normal eye. The layers have been labeled as: ILM: inner limiting membrane, RNFL: retinal nerve fiber layer, GCL+IPL complex: ganglion cell layer and inner plexiform layer, INL: inner nuclear layer, OPL: outer plexiform layer, ONL: outer nuclear layer, OS: outer segment of photoreceptors, and retinal pigment epithelial layer (RPE). We note that the sublayer labeled as ONL is actually enclosing the external limiting membrane (ELM) and IS, but in the standard 10 µm resolution OCT image this thin membrane cannot be visualized clearly, making the segmentation of the IS difficult. Therefore, this layer classification is our assumption and does not reflect the actual anatomic structure. Also, observe that since there is no significant luminance transition between GCL and IPL, the outer boundary of the GCL layer is difficult to visualize in the Stratus OCT image shown. Thus, a combined GCL+IPL layer is preferable.

also on the classification of neighbouring pixels. These local correlations provide a mechanism for modeling a variety of image properties (Li, 1995). MRF is often incorporated into clustering segmentations such as *K*-means under a Bayesian prior model (Held et al., 1997; Pappas et al., 1992; Rajapakse et al. 1997).

3. *Pattern recognition methods*: Since structures in medical images can be considered as patterns, pattern recognition techniques can be used in segmentation procedures. There are supervised and unsupervised classification methods used to perform segmentation. Supervised classification algorithms are pattern recognition techniques that require training data that are manually segmented and then used as references for automatically segmenting new data. Typical supervised algorithms include artificial neural network (ANN), support vector machine (SVM) and active appearance models (AAM) (Alirezaie et al., 1997; Cootes et al., 2001; Wang et al., 2001). Unsupervised classification algorithms, also known as clustering algorithms, do not require a training set but they do require initial parameters to perform segmentation. Commonly used unsupervised classification algorithms include Fuzzy C-means algorithm (FCM), iterative self-organizing data analysis technique algorithm (ISODATA) and unsupervised neural network (Cheng et al., 1996; Mohamed et al., 1998; Wong et al., 2002).

4. *Deformable model methods*: These are model-based techniques for delineating region boundaries using closed parametric curves or surfaces that deform under the influence of internal and external forces. Deformable models can be classified into parametric and geometric models depending on the contour representation. These algorithms are usually interpreted as a modeling of curve evolution because they delineate an object boundary in an image by placing a closed curve or surface near the desired boundary and then allowing to undergo an iterative relaxation process. The parametric deformable models sample contours as discrete points and track them according to their respective moving equations. The moving equation for the parametric deformable models can be derived through either energy functional or dynamic forces. A priori knowledge can be easily incorporated to the procedures of parametric models. The geometric deformable models are based on the level set method (Osher & Sethian, 1988), which embed the moving contour into a higher dimensional level set function and view the contour as its zero level set. Then, instead of tracking the contour points, the zero level set of the level set function are tracked. The advantage of doing so is that topological changes can be naturally handled and the geometric properties of the contour such as normal vector and curvature can be calculated implicitly. Consequently, the computational complexity is decreased.

5. *Global optimization methods*: A growing number of image segmentation approaches use energy minimization techniques (Boykov & Funka-Lea, 2006; Kolmogorov & Zabih, 2004). Among all the various energy minimization techniques for segmentation, graph cuts are based on partitioning a graph by a minimum cut / maximum flow optimization algorithm (Greg et al., 1986; Ford & Fulkerson, 1956). The image is represented using an adjacency graph. Each vertex of the graph represents an image pixel, while the edge weight between two vertices represents the similarity between two corresponding pixels. Usually, the cost function to be minimized is the summation of the weights of the edges that are cut.

6. *Registration Methods*: The standard method used is the atlas-guided approach which treats segmentation as a registration problem (Maintz & Viergever, 1998). Typically, the atlas is generated by compiling information on the anatomy that requires segmentation

and then used as a reference frame for segmenting new images. This approach is theoretically similar to classifier methods but it is implemented in the spatial domain of the image rather than in a feature space. This approach uses a procedure known as atlas warping which first finds a one-to-one transformation that maps a pre-segmented atlas image to the target image that requires segmenting. The warping can be performed using linear transformations (Andreasen et al., 1996; Lancaster et al., 1997; Talairach and P. Tournoux, 1988).

7. *Model-fitting methods*: These approaches usually fits a simple geometric shape such as an ellipse or parabola to the locations of extracted image features in an image (Pathak et al., 1998). It is a technique which is specialized to the structure being segmented but is easily implemented and can provide good results when the model is appropriate. A more general approach is to fit spline curves or surfaces to the features (Kim & Hori, 2000).

8. *LEGION based*: These approaches are a biologically plausible computational framework for image analysis based on a biologically inspired oscillator network, called the locally excitatory globally inhibitory oscillator network (LEGION) (von der Malsburg, 1981;
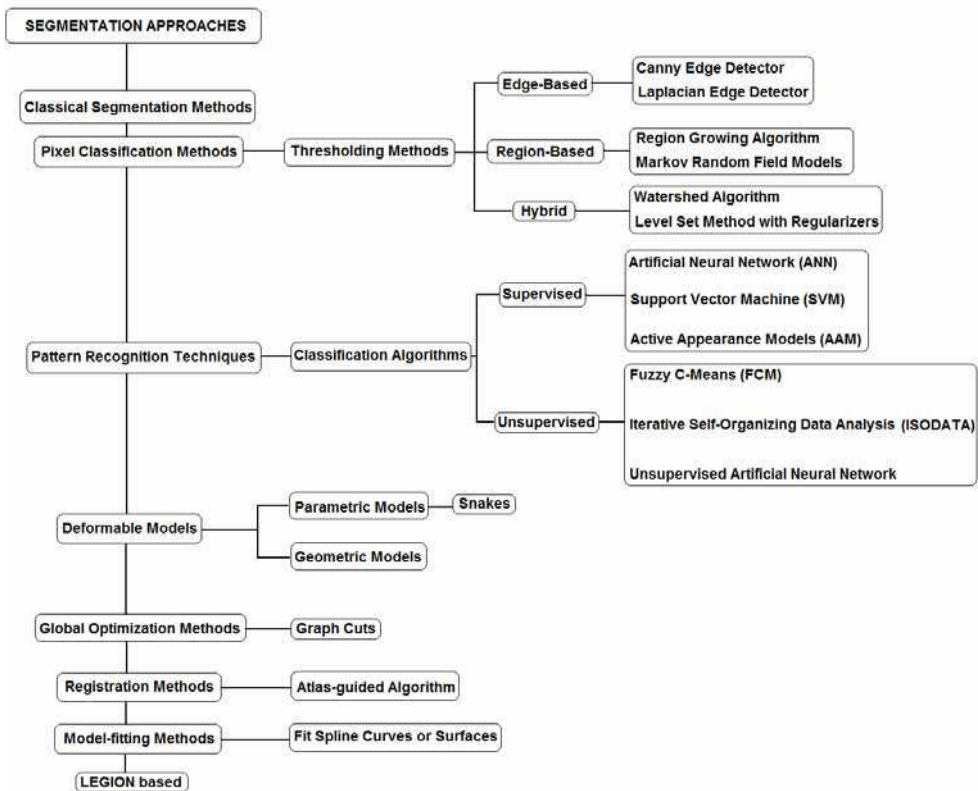

Fig. 10. Classification of segmentation approaches.

Wang & Terman, 1995; Wang & Terman, 1997). The network was proposed based on theoretical and experimental considerations that point to oscillatory correlation as a representational scheme for the working of the brain. The oscillatory correlation theory assumes that the brain groups and segregates visual features on the basis of correlation between neural oscillations (von der Malsburg, 1981; Wang & Terman, 1995).

As a final point, it is noteworthy to mention that years of research in segmentation have demonstrated that significant improvements on the final segmentation results may be achieved by using notably more sophisticated feature selection procedures, more elaborate segmentation techniques, taking into account prior distribution on the labels, region processes, or the number of classes, finally, involving (e.g. in the case of energy-based segmentation models) more costly optimization techniques.

5. Review of algorithms for segmentation of retinal image data using OCT

In opthalmology, a number of segmentation approaches of retinal image data using OCT have been proposed to enhance the clinical benefit of the OCT technology in the process of clinical decision making. The success of OCT in the investigation and treatment of retinal diseases might be best illustrated by the progress in automated analysis and the recent advancement of this technology from time domain to spectral domain (Cense et al., 2004; Drexler & Fujimoto, 2008; Fercher et al., 1995; Huang et al., 1991; Wojtkowski et al., 2003). The segmentation of the retinal structure is a challenging topic that faces major problems. First, OCT images suffer from the intrinsic speckle noise, which decreases the image quality and complicates the image analysis. This particular noise is the foundation of existing problems in the precise identification of the boundaries of the various cellular layers of the retina and other specific retinal features present in the OCT tomograms. Second, since the intensity pattern in OCT images results from absorption and scattering of light in the retinal tissue, intensity of a homogeneous area decreases with increasing imaging depth deterministically. This complicates segmentation algorithms which are commonly based on the assumption that intensity variations of homogeneous regions are only due to noise and not intrinsic to the imaging modality. The third problem is the low optical contrast in some regions of the OCT images due to the optical shadows of the retinal blood vessels resulting from the high haemoglobin absorption of light. Finally, motion artifacts and sub-optimal imaging conditions affecting the quality of the OCT tomograms also cause failure in the segmentation approaches or reduce their accuracy.

In this section, a number of approaches that have appeared in the literature on OCT image segmentation are described. This review concentrates on automated and semi-automated algorithms developed to segment the various cellular layers of the retina, structural irregularities associated to retinal disease (e.g. drusen and fluid-filled regions), and particular features of the optic nerve head in OCT images. Specifically, automation in OCT image analyses requires the establishment of parameters and features obtained from quantitative measurements of OCT data such as optical and structural parameters, scattering properties and refractive index of biological tissues. Thus, Table 1 gives an overview of the approaches discussed in this section based on the details of the above quantitative parameters and features. Although retinal blood vessel segmentation methods often consist of applying segmentation algorithms to fundus images, and more recently to

advanced OCT images (e.g. SDOCT and UHR OCT) using the vessel shadows (Wehbe et al., 2007), I consider this application of segmentation to be a separate branch of research and do not included it in this review. The segmentation methods that will be reviewed can be classified into three groups based on the dimension (D) of the image analyzed. In particular, a number of different methods have been reported under the 1D, 2D and 3D categories (see Table 1). Segmentation approaches of OCT retinal images differ depending on the number of retinal features (e.g. number of intraretinal layers and fluid-filled regions) to be segmented, and on their robustness in the presence of inherent speckle noise, retinal blood vessel shadows and structural irregularities at the fovea, macula and optic nerve in pathological retinal tissue. Most of the initial segmentation algorithms are based on information retrieved from either gradient or conventional intensity data. However, some recent segmentation methods are based on more complex models, such as active contours and optimal graph search methods. It is worthy of mention that all existing published segmentation approaches have been basically introduced to overcome the limitation of the commercial OCT softwares and most of them have provided additional quantitative information of the retinal structure.

As it can be seen in Table 1, a number of segmentation approaches have been proposed to segment the retinal structure. The initial segmentation method proposed by Hee *et al.* was based on intensity variation and demonstrated the potential of OCT as a quantitative tool to measure total retina and RNFL thickness (Hee et al., 1995a, 1995b; Hee, 1997). This very first method used a 1D edge detection kernel approach, which is independent of the absolute signal level in the image, to compute the derivative of reflectivity versus axial distance for each A-scan in the OCT image. Thus, it is more effective than threshold identification. Specifically, the detection kernel identified the strongest two edges in each A-scan using peak-detection in more than 90% of the A-scans. Huang *et al.* used a similar approach to characterize the retina and outer retina choroid complex in hereditary retinal degenerations in experimental animals and humans (Huang et al., 1998). This early work, to the knowledge of the author, represents the first study to characterize and quantify OCT signals in relation to the optical properties of retinal layers. In contrast, George *et al.* used a dual threshold to segment the retina and choriocapillaries structure from OCT images (George et al., 2000). Unfortunately, very little information is available about this work. However, simple thresholding is sensitive to noise and intensity inhomogeneities in OCT images because it does not take into account the spatial characteristics of the image. Koozekanani, *et al.* introduced a Markov random field (MRF) model for extracting the inner and outer retinal boundaries from radial scans of the macula (Koozekanani et al., 2001). This autoregressive model showed to be more robust on the macular region of normal retinas than standard column-wise thresholding methods. Particularly, retinal thickness was calculated with an error comparable to the 10μm resolution of the OCT system used, representing a substantial improvement over clinical measurements provided by the Humphrey 2000 OCT built-in algorithm. Although a difficulty associated with MRF models is the proper selection of parameters controlling the strength of spatial interactions, Koozekanani's model is entirely independent and involves no critically tuned parameters. However, the main problem of this model is to find reliable "seed" points for OCT images of retinal pathologies. On the other hand, since this model relies on simply connecting 1D points, makes it sensitive to

noise. Thus, it demands to apply special rules to correct for errors in the extracted layer borders because the model per se is sensitive to noise.

Since the problem with thresholding lies in the selection of the threshold, Herzog *et al.* proposed a method based on edge maximization and smoothness constraints to choose an optimal threshold to utomatically extract the optic nerve and retinal boundaries from axial OCT scans through the optic nerve head (ONH) (Herzog et al., 2004). A method to automatically segment the curve to extract the nerve head profile was also proposed. An interesting aspect is that in this approach the boundaries are obtained by maximizing the number of edges that lie on the boundary while minimizing the boundary's average rate of change. The algorithm generally identified the correct vitreal-retinal boundary in the images except in regions where the OCT signal was severely attenuated due to shadowing. This study is the first published work on ONH segmentation using TDOCT data. Two years later, a more efficient methodology to segment OCT nerve head images and extract the necessary parameters for clinical measurements such as the cup-to-disk ratio and RNFL thickness was proposed by Boyer *et al*. (Boyer et al., 2006) The improved methodology is esentially a parabolic model of the cup geometry and an extension of the Markov model introduced by Koozekanani *et al.* This study is the first published work on clinical parameter extraction taking advantage of the optic nerve head cross-sectional geometry in TDOCT images. Recently, Shrinivasan *et al.* also used a modification of the Koozekanini algorithm to perform quantitative measurements of the outer retinal morphology using UHR OCT (Shrinivasan et al., 2008). In this study the thick scattering region of the outer retina previously attributed to the RPE is shown to consist of distinct scattering bands corresponding to the photoreceptor outer segment tips, RPE, and Bruch's membrane.

Gregori *et al.* presented the first algorithm that was able to locate automatically and/or interactively the complex geometry and topology typical of many macular pathologies in TDOCT images (Stratus OCT system), and lately in SDOCT images (Cirrus HD-OCT unit) (Gregori et al., 2004; Gregori et al., 2005; Gregori et al., 2008). Unfortunately, this is a proprietary algorithm that has not been described in detail because has been licensed to Carl Zeiss Meditec, and it is currently part of the commercial Cirrus HD-OCT instrument. However, it is a robust algorithm able to locate the boundaries of the major anatomical layers internal to the retina with great accuracy not only in eyes presenting abnormal and unusual anatomy but also in poor quality images. Table 1 includes a summary of all the results that have been presented in the ARVO meetings since 2004.

In 2005, algorithms based only on intensity variation were also presented (Shahidi et al., 2005; Ishikawa et al., 2005; Cabrera Fernández et al., 2005b). In general, these algorithms overcame the limitations of the commercial OCT3/Stratus OCT software and also provided additional quantitative information. For example, Shahidi *et al.* segmented three retinal segments by using a simple search of peaks corresponding to high- and low-intensity bands, and an improved edge detection approach using the correlation between axial A-scans was presented in a more recent study (Bagci et al., 2007). Ishikawa *et al.* used a modified median filter and an adaptive thresholding method based on the reflectivity histogram of each A-scan line to segment four layer structures within the retina (Ishikawa et al., 2005). A similar adaptive thresholding approach along with an intensity peak detection procedure was also employed by Ahlers *et al*. to segment data from patients with RPE detachments (Ahlers et

al., 2008). This study was also based on the work by Gregori *et al.* (Gregori et al., 2005). It is worthy of mentioning that the work of Ishikawa *et al.* was the first report demonstrating that the thickness of the innermost layers in the macula had diagnostic power comparable with that of circumpapillary nerve fib er layer (cpNFL) in glaucoma studies (Ishikawa et al., 2005). Later on, Tan *et al. using* a 2D gradient approach in a dynamic programming framework also confirmed that glaucoma primarily affects the thickness of the inner retinal layers (RNFL, GCL, IPL) in the macula (Tan et al., 2008). Cabrera Fernández *et al.* used complex diffusion filtering to reduce speckle noise without blurring retinal structures and a peak finding algorithm based on local coherence information of the retinal structure to determine seven intraretinal layers in a automatic/semi-automatic framework (Cabrera Fernández et al., 2005b). This algorithm searches for edges in a map obtained by calculating the first derivative of the structure coherence matrix using the denoised image. Although, good results were obtained for some pathological Stratus OCT images, the algorithm in its original development was prone to failure and allowed detected boundaries to overlap. This algorithm worked reliably for data from 72 OCT B-scans from healthy normal subjects. The automatic/semi-automatic framework developed by Cabrera Fernández *et al.* was used to demonstrate for the first time the potential of OCT quantification for early DR damage (Cabrera Fernández et al., 2008; Cabrera DeBuc et al., 2010). The early segmentation work of Gregori *et al.*, Ishikawa *et al.* and Cabrera Fernández *et al.* allowed the automated generation of 2D thickness maps of individual retinal layers and, therefore, also a more local analysis of the retinal morphology using Stratus OCT data before the introduction of advanced OCT systems (Gregori et al.,2005; Ishikawa et al., 2005; Cabrera Fernández et al., 2005b).

A different approach using active contour algorithms has been used to quantify structural irregularities in OCT retinal images. For example, Cabrera Fernández *et al.* applied for the first time a deformable model to TDOCT images of retinas demonstrating cystoids and subretinal fluid spaces using a semi-automatic framework (Cabrera Fernández et al., 2004; Cabrera Fernández et al., 2005a). Specifically, this method used a nonlinear anisotropic diffusion filter to remove strong speckle noise and a gradient vector flow (GVF) snake model to extract fluid-filled regions in the retinal structure of AMD patients. Extension of this deformable model framework to a daily routine image analysis might prove to be difficult and unpractical since the algorithm requires manual interaction to place an initial model and choose appropriate parameters. Mujat *et al.* used deformable splines to assess the thickness of the RNFL in SDOCT images. (Mujat et al., 2005). Although all the model parameters were set based on a large number of OCT scans in different retinal areas, contour initialization is still a major problem because it must be close to the true boundary locations. In addition, though sensitivity to initialization was not reported in this study, the approach was highly vulnerable to the existence of blood vessels and other morphological retinal features. However, the advantage of this automated snake methodology is that it is able to provide larger area maps of the RNFL thickness facilitating the correct registration of ROIs with visual field defects which could allow better longitudinal evaluation of RNFL thinning in glaucoma studies. In 2009, Yazdanpanah *et al.* presented a modified Chan–Vese's energy-minimizing active contour algorithm in a multi-phase framework to segment SDOCT data from rodent models. This approach incorporated a circular shape prior based on expert anatomical knowledge of the retinal layers, avoiding the need for training

(Yazdanpanah, et al., 2009). Although the sensitivity of the algorithm with respect to model parameters and initialization was not tested, the experimental results showed that this approach was able to detect with good accuracy the desired retinal layers in OCT retinal images from rats compared to the ground truth segmentation used in the evaluations performed. Moreover, the algorithm was not evaluated for images including the foveal pit. Later on, Mishra *et al.* also presented a modified active contour algorithm based on a sparse dynamic programming method and a two-step kernel based optimization scheme (Mishra et al., 2009). Although this effective algorithm achieves accurate intra-retinal segmentation on rodent OCT images under low image contrast and in the presence of irregularly shaped structural features, results on images including the foveal pit region were not given and no quantitative evaluation using a large data set was provided.

Baroni *et al.* used a multi-step approach to extract the boundaries of the vitreo-retinal interface and the inner and outer retina by maximizing an edge likelihood function (Baroni et al., 2007). Interestingly, the effect of intravitreal injection of triamcinolone acetonide for the treatment of vitreo-retinal interface syndrome was evaluated using a set of measures such as thickness measurement, densitometry, texture and curvature extracted from the identified retinal layers. This study was the first report, to the knowledge of the author, that demonstrated the potential of texture information in TDOCT retinal images as a complimentary information of retinal features to aid diagnosis. Another intensity variation based approach to segment the posterior retinal layers, which is resistant to discontinuities in the OCT tomogram, was presented by Szulmowski *et al* (Szulmowski et al., 2007). Furthermore, the quantitative analysis has been largely limited to total retinal thickness and/or inner and outer retinal thickness in early studies exploring the correlation between histology and OCT in rodents (e.g. see Kocaoglu et al., 2007 & Ruggeri et al., 2007). Recently, more intensity variation based approaches have also been presented (see Table 1 for details) (Fabritius et al., 2009; Tumlinson et al., 2009; Koprowski et al., 2009 ; Lu et al., 2010 and Yang et al., 2010) Among them, it is worthy to mention that Fabritius *et al.* incorporated 3D intensity information to improve the intensity based segmentation and segmented the ILM and RPE directly from the OCT data without massive pre-processing in a very faster manner. (Fabritius et al., 2009). Likewise, Yang *et al.* presented a fast, efficient algorithm that simultaneously utilized both local and global gradient information (Yang et al., 2010). This approach skillfully used an A-scan reduction technique to reduce the execution time to 16 seconds per volume (480x512x128 voxels) without remarkably degrading the accuracy or reproducibility of the results. In addition, an alternative promising method was introduced by Mayer *et al.*, who used a fuzzy C-means clustering technique to automatically segment RNFL thickness in circular OCT B-scans without the need of parameter adaptation for pathological data (Mayer et al., 2008).

In contrast to the edge detection approaches mentioned above, a multi-resolution hierarchical support vector machine (SVM) was used in a semi-automatic approach to calculate the thickness of the retina and the photoreceptor layer along with the volume of pockets of fluid in 3D OCT data (Fuller et al., 2007). In this approach, the SVM included scalar intensity, gradient, spatial location, mean of the neighbors, and variance. Although this SVM method performed well on both healthy and diseased OCT data, a major drawback was that some voxels were mis-classified resulting in scattered noise in the thickness maps. In addition, this method requires that the user paints the areas of interest in

any slice of the volume. Thus, the training data set grows through painting increasing the complexity of the SVM, and as a result more time is required to complete the segmentation task. A different approach was presented by Tolliver *et al.*, who used a graph partitioning algorithm that assumes that different regions of the OCT image correspond to different modes of oscillation. The oscillation steps that represent the retinal edges are then determined by an eigenvector calculation (Tolliver et al., 2008). By using the eigenvector from the prior step as a starting point, for finding the new eigenvector, the approach works in only a small number of steps. In this study, the accuracy range for the detected boundaries was good and the algorithm performed well in the presence of retinal pathology. On the contrary to the vast majority of the studies cited so far, Götzinger *et al.* used PS-OCT to segment the RPE layer employing polarization scramble features. Even though the two algorithms presented facilitated a better visualization and quantification of RPE thickening and RPE atrophies when compared to algorithms based on intensity images, a PS-OCT system is needed to acquire polarization data (Götzinger et al., 2008).

A more complex approach to OCT retinal layer segmentation using gradient and/or intensity information in a 3D context was presented by Haecker *et. al.*, who generated a composite 3D image from radial linear TDOCT 2D scans and performed a 3D graph-search (Haecker et al., 2006). The basic idea of this graph approach is to break a graph into paths or fragments, which are utilized as filtering features in graph search. The early development of Haecker *et al.*'s algorithm extracted only 2 intratretinal layers and was evaluated on data from 18 controls and 9 subjects with papilledema (Haecker et al., 2006). This approach was further developed into a multilayer segmentation (Garvin et al., 2008) showing superior results for high quality OCT data. This graph-search approach potentially increased the accuracy of segmentation by using weights describing both edge and regional information to segment the volume. However, assumptions on the layers, as Garvin *et. al.* made, may be violated in pathological cases, or parameters have to be adapted for either normal subjects or pathological patients. Even though this elegant method can guarantee to find the global minimums when compared to deformable models, its computational complexity can really increase the computation time if more complex constraints are required to segment diseased retinal images showing common structural irregularities and a less ideal foveal pit. In 2009, Abramoff *et al.* combined a multiscale 3D graph search algorithm and a voxel column classification algorithm using a k-NN classifier to segment the ONH cup and rim (Abramoff, et al., 2009). This preliminary study showed for the first time a high correlation between segmentation results of the ONH cup and rim from SDOCT images and planimetry results obtained by glaucoma experts on the same eye. Later on, Lee *et al.* presented an improved and fully automatic method based on a similar methodology using graph search combined with a k-NN classifier that employed contextual information combined with a convex hull-based fitting procedure to segment the ONH cup and rim (Lee et al., 2010). In general, the methodology showed good performance but additional processing steps to compensate for the presence of vessels in and around the ONH would be required to reduced misclassified A-scans on the vessels and increase the accuracy of the ONH rim or cup contour segmentation. Similarly, Hu *et al.* used a graph-theoretic approach to segment the neural canal opening (NCO) and cup at the level of RPE/Bruch's membrane complex (Hu et al., 2010). Qellec et al. presented a promising method for detecting footprints of fluid-filled regions in SDOCT images from AMD patients (Quellec et al., 2010). This approach also used

a multiscale 3D graph search method to identify automatically a total of 10 intraretinal layers. The segmented layers were characterized by their thickness and 3D textural features. As in the Baroni et al. study, this report confirmed that useful 3D textural information can be also extracted from SDOCT scans to aid local retinal abnormality detection. In addition, Chiu *et al*. reported a skillful approach based on graph-based theory and dynamic programming that significantly reduced the processing time required for image segmentation and feature extraction (Chiu et al., 2010). This methodology is able to address sources of instability such as the merging of layers at the fovea, uneven tissue reflectivity, vessel hypo-reflectivity and the presence of pathology. Interestingly, the approach incorporates an automatic initialization that bypasses the need for manual endpoint selection.

The development of SDOCT systems has also made possible a better visualization and identification of the RPE-Bruch's membrane providing the ability to image drusen. As a result, segmentation algorithms have been recently presented to quantify drusen area and volume in AMD patients. For example, Farsiu *et al*. presented the DOCTRAP algorithm that is based on a modified implementation of the GVF snake model to accurately segment drusen in SDOCT images of AMD eyes (Farsiu et al., 2008). This methodology also included a semi-supervised approach to correct for segmentation errors such as false regions marked as drusen in images showing RPE elevation unrelated to drusen. The approach presented by Fuller *et al*. and described above also facilitates the semi-automatic segmentation of drusen in SDOCT images (Fuller et al., 2007). Gregrori *et al*. has also measured drusen area and volume using quantitative descriptors of drusen geometry in three dimensional space (Gregori et al., 2008). In addition, Yi *et al*. characterized ONH drusen using a commercial available software (see Table 1 for details) (Yi et al., 2009).

Kajić *et al*. presented a promising novel statistical model based on texture and shape able to capture the variance of the training data used to segment unseen data (Kajic et al., 2007). As the authors themselves stated, this guarantees that the segmentation will be close to the ground truth and less sensitive to noise. This algorithm successfully segments 8 intraretinal layers on 3D OCT data even under conditions which prove extremely difficult for some pre-existing segmentation approaches cited in the literature. It also has the potential of segmenting choroid layers and the ONH. In this study, for the first time, an error measure is computed from a large manually segmented data set which was certainly segmented twice by different operators.

6. Concluding remarks

In contrast to OCT technology development which has been a field of active research since 1991, OCT image segmentation has only being fully active explored during the last decade. However, it continues to be one of the more difficult and at the same time most commonly required steps in OCT image analysis, therefore, there does not and can not exist a typical segmentation method that can be expected to work equally well for all tasks. The works cited in this review spread from the 1997's until September 2010. Of course, the citation in this review is by no means complete. For example, an early active research topic such as manual tools for image segmentation has not been covered. It is also worthy the mentioning that it was difficult to assess the robustness of the various segmentation approaches because of many authors have used different OCT imaging setups and reported limited quantitative

validation. Accordingly, a careful evaluation of different available academic and commercial segmentation methods using common test datasets is required to choose the one that best solves the given image processing task.

Current research in the segmentation of OCT images is striving towards improving the accuracy, precision, and computational speed of segmentation methods, as well as reducing the amount of manual interaction. On the other hand, most of the reported computation times of segmentation methods on 2D and 3D OCT datasets (see Table 1) are not really practical for general clinical use. However, segmentation methods will be particularly valuable in areas such as computer assisted surgery, where real-time visualization of the anatomy is a crucial component. For increasing computational efficiency, multiscale processing and parallelizable methods appear to be promising approaches (Sylwestrzak et al., 2010). As a matter of fact, the current expanding use of 3D OCT systems along with the advances in volume rendering techniques, is now shifting slowly the focus of segmentation to volume segmentation. In addition, the potential of OCT image segmentation to evaluate therapeutic or adverse effects of experimental interventions in time-course experiments might prove to be even more important to translate insights from bench to bedside in a proficient and timely manner.

Since OCT allows real-time data acquisition, future research will strive towards improving automation and data evaluation in near real time to support retinal disease screening and diagnosis. Automated segmentation still remains one of the most difficult problems in the world of OCT retinal image segmentation. This dificulty mainly arises due to the sheer size of the datasets coupled with the complexity and variability of the pathological retinal anatomy. The situation is worsened by the shortcomings of OCT imaging systems, such as sampling artifacts, noise, low contrast etc. which may cause the boundaries of retinal structures to be indistinct and disconnected. Recently, Liu *et al.* introduced a very effective approach for automated macular pathology identification in retinal OCT images (Liu et al., 2010). This method uses a machine learning approach that has the potential to provide unsupervised objective classifications for automated OCT data analysis in real time. Computational efficiency is particularly important in real-time processing applications for computer aided diagnosis and surgical planning. As a matter of fact, segmentation algorithms do have the capability to run in parallel with the OCT scanning method and to provide a concrete support for clinical decision making in real time.

Finally, it is worthy of mention that automated segmentation methods will never replace physicians but they will likely become crucial elements of medical image interpretation. Thus, there are numerous challenges to improve clinical decision making based on automated processing of OCT data, as outlined throught this chapter, for engineers, mathematicians, physicists and physicians working to advance the field of OCT image analysis.

7. Acknowledgement

First Author/Year/ OCT system	Feature Studied	Sample Size	Preprocessing	Segmentation Method	Automation	Error Correction/ Refinement Method	Validation (key points)	Remark	Computation Time
Hee, MR., 1997/ TDOCT (Humphrey 2000 OCT)	Retinal and RNFL thickness	Imaging data from various pathological retina	Low-pass filtering: 2D center-weighted kernel	1D edge-detection kernel/peak-detection approach	Automated	Interpolation and local edge-detection	Reproducibility of the RNFL thickness in 10 glaucomatous eyes	First report of image processing techniques and methods of extracting quantitative information from OCT images	Not reported
Huang, Y., 1998, TDOCT (Humphrey 2000 OCT)	Thickness of the retina and outer retina choroid complex (ORCC=photoreceptor layer+RPE+anterior choroid); and the reflectivity posterior to ORCC	OCT data from human subjects (normal & with hereditary retinal degenerations) and degenerative avian and swine retinas	2D lineal smoothing (3x3 center-weighted Gaussian smoothing filter applied 5 times)	Algorithm based on signal amplitude and slope calculated using a 1st-derivative weighted filter	Automated	None	Not reported	First report of quantitative OCT results in hereditary retinal degenerations in experimental animals and humans	Not reported
George, A., 2000/ TDOCT (Humphrey 2000 OCT)	Thickness and volume of the retina and choriocapillaries	Information not available(I/N/A)	Median filter and image homogenization using Nagao filter	Dual threshold to segment the retina and choriocapillaries structures	Automated	(I/N/A)	(I/N/A)	(I/N/A)	(I/N/A)
Koozekanani, D., TDOCT (2001, Humphrey 2000 OCT)	Inner and outer borders of the retina	1450 images (B-scans)	4x4 median filter (applied twice)	1D edge detection kernel/Markov Boundary Model	Automated	Manual correction for evaluation purposes and linear interpolation to correct segmentation errors	Automatic and manual measurements differed by less than 25 μm, and in 89% of the tests the difference was less than 10 μm (near the resolution limit)	Algorithm offered performance significantly superior to the Humphrey 2000 OCT's built-in algorithm	Not reported
Herzog, A., 2004, TDOCT (Humphrey 3000 OCT)	ONH and retinal boundaries from axial OCT scans through the ONH	Exemplary OCT B-scans taken at the ONH	Median filter (4x4 applied twice)	Adaptive threshold algorithm based on edge maximization and smoothness constraints	Automated	None	None	First published results on ONH segmentation and geometric characterization from OCT data	Not reported
Gregori, G., 2004-, TDOCT (Stratus OCT) and SDOCT	Global boundaries (ILM, RPE),	Stratus OCT: 40 OCT B-scans	Non-linear anisotropic filter	Iterative boundary detection	Automated /Semi-Automated	None	Agreement with boundaries determined by	First segmentation algorithm that was able to locate	Not reported

(Cirrus HD-OCT)	NFL, GCL+IPL, boundaries of epiretinal membranes and other vitreous structures, the boundaries of cystic spaces, drusen, and RPE detachment	SDOCT: 150 eyes (full range of retinal diseases), 30 glaucomatous eyes and 30 normal eyes	(Structural Correlation Algorithm for Speckle Removal (SCASR))	algorithm			visual inspection agreed on at least 99% of the pixels and never diverges by more than 10% of the correct local retinal thickness. Automated detected boundaries were within 20 microns from manually drawn boundaries on well over 90% of pixels	automatically and/or interactively the complex geometry/topology typical of many macular pathologies.	
Shahidi, M., 2005, TDOCT (OCT3 Carl-Zeiss Meditec)	Thickness of the total retina and 3 retinal segments	OCT data from 10 healthy subjects	Median filter	Peak search algorithm (simple search of peaks corresponding to high- and low-intensity bands)	Automated	None	Reproducibility of thickness measurements showed that changes of 28 to 36 μm can be detected with 95% confidence	Algorithm averaged thickness profiles in the transversal direction producing less refined thickness profiles	Not reported
Ishikawa, H., 2005, TDOCT (Stratus OCT)	Various retinal layers/segments (4)	Forty-seven subjects (23 normal and 24 with glaucoma)	Modified mean filter (kernel size 7x5)	Adaptive thresholding technique (cutoff threshold was calculated based on reflectivity histogram of each A-scan line)	Automated	None	Algorithm failure of at least one detected border in approximately 10% of the good-quality images.	First segmentation algorithm that demonstrated the thickness of the innermost layers in the macula had diagnostic power comparable with that of cpNFL.	Not reported
Cabrera Fernández, D., 2005, TDOCT (Stratus OCT)	Cystoids and subretinal fluid-filled regions	OCT images from 7 patients with AMD	Nonlinear anisotropic diffusion filter	Gradient vector flow snake model	Semi-Automated	Manual correction for evaluation purposes	Mean distance between all extracted contours using the snake algorithm and the expert's contours was below 3 pixels.	First deformable model applied to OCT images of AMD patients demonstrating cystoids and subretinal fluid spaces.	84-92 seconds (on average) for a set of six radial OCT B-scans in a Pentium 4 CPU, 2.26 GHz
Mujat, M., 2005, experimental SDOCT	RNFL thickness	Two volumetric data sets of the same eye from a single subject	Anisotropic filtering	Deformable splines (snake algorithm)	Automated	None	Algorithm performed well in 350 frames with only few and isolated boundary detection errors	Provided large area maps of the RNFL thickness facilitating the correct registration of ROIs in glaucoma longitudinal studies	62 seconds for a single image (1000 A-scans) on a 3.2 GHz Pentium 4 processor

Cabrera Fernández, D., 2005, TDOCT (Stratus OCT)	Various retinal layers/segments (7)	72 OCT B-scans from normal subjects and 4 B-scans from pathological eyes	Complex diffusion filter	OCTRIMA software which uses a peak search algorithm based on local coherence information of the retinal structure.	Automated /Semi-Automated	Manual correction to eliminate segmentation pitfalls (if any) during the automatic procedure	All instances of algorithm failure were in regions which had extremely low reflectivity or almost no structural information.	First segmentation algorithm that demonstrated the potential of OCT's quantification for early DR damage.	24 seconds for filtering-segmenting each OCT B-scan (1024x512-pixel) on a personal computer (Pentium 4 CPU, 2.26 GHz).
Boyer, K., 2006, TDOCT (OCT 3000 Zees-Humphrey)	ONH (cup-to-disk ratio) and RNFL thickness	OCT data from 59 axial OCT nerve head scans	2D median filter (4x4 applied twice) along with a Palladian of Gaussian (1D) edge detector	Parabolic model of cup geometry and an extension of the Markov model introduced by Koozekanani, *et al.* to segment the retinal-nerve head surface, identify the choroid-nerve head boundary, and the extent of the optic cup	Automated	A glaucoma specialist marked the cup end points in 59 images in order to compare cup endpoints selected by the ophthalmologist to those selected automatically by the algorithm.	A correlation coefficient for cup diameter above 0.8 and above 0.9 for the disk diameter	First published results on clinical parameter extraction taken advantage of the ONH cross-sectional geometry in OCT images	Total processing time of 9.42 seconds (7.62 seconds for extracting the retinal-vitreal boundary requires, 0.793 seconds segmenting the cup limits, and 1.004 seconds for segmenting the disk limits) on a Pentium M, 1.8 GHz processor with 1 GByte of RAM
Baroni,M., 2007, TDOCT (OCT2 Carl-Zeiss Meditec)	ILM, RNFL, inner retina (IR), including GCL and IPL; and outer retina (OR), including OPL and inner photoreceptor layers (IPL)	16 pathologic OCT images from patients with crinkled cellophane maculopathy	Two 1D filters were used: 1) median filtering (5 pixels) along the A-scans; 2) Gaussian kernel in the longitudinally direction	2D dynamic programming where edge detection uses a Gaussian gradient applied cross-sectionally, as a 1D filter (detection of peaks using cumulative horizontal histograms and boundaries obtained by	Automated	None	None	First multi-step segmentation approach that demonstrated the potential of texture information in TDOCT images as a complimentary information of retinal features to aid diagnosis	Not reported

				maximizing an edge likelihood function)					
Szkulmowski, M., 2007, experimental SDOCT	Posterior retinal layers	OCT data from normal eyes and eyes with a selection of retinal pathologies	None	Variation of a multiple thresholding algorithm that identifies regions in the tomogram that have similar intensity and variance	Semi-Automated	Evaluation of the quality of segmentation requires operator intervention.	Not reported	Segmentation method is resistant to discontinuities in the tomogram	About 5 minutes for full processing of a data volume containing 200 images with 600 A-scans/image on a personal computer with a Pentium 4, 2 GHz processor
Ruggeri, M., 2007, experimental SDOCT	ILM, RPE layers along with tumor volume in small animals	OCT data from normal and diseased rodent eyes	Not reported	3D segmentation algorithm that detects the ILM and RPE boundaries by means of an iterative procedure by which an initial guess is repeatedly evaluated and improved	Automated for extracting the inner and outer borders of the retina. Manual segmentation was performed on each cross-sectional OCT image to obtain the boundaries of the tumor in the retinoblastoma model.	None	None	Algorithm facilitates the thickness map of the rodent retina	Not reported
Fuller, AR., 2007, experimental 3D OCT	Thickness of the retina and the photoreceptor layer along with the volume of pockets of fluid	Data from patients with AMD and retinal detachment	Noise is handled by considering voxel's mean value and variance across multiple resolutions in the SVM approach	Multi-resolution Hierarchical Support vector machine (SVM)	Semi-Automated	Manual segmentation tool for evaluation purposes	68% of the thickness differences between the SVM segmentation and the manual segmentation fell below 6 voxel units	SVM approach with global awareness by considering statistical characteristics at multiple levels of resolution	Less than two minutes (on average) for the full thickness segmentation performed on a computer with 3GB of RAM (dual processor 3GHz Intel Xeon)

Tan, O., 2008, TDOCT (Stratus OCT)	Various retinal layers/ segments	149 glaucomatous patients and 47 normal patients	Gaussian smoothing filtering	Gradient approach using dynamic programming (2D approach)	Automated	Progressive segmentation	Repeatability of thickness measurements showed the potential of using the thickness of both retina and inner retinal layers for tracking glaucoma progression.	Segmentation results confirmed that glaucoma primarily affects the thickness of the inner retinal layers (RNFL, GCL, IPL) in the macula.	Not reported
Garvin, M., 2008, TDOCT (Stratus OCT)	Various retinal layers/ segments (5)	OCT data from 12 patients (24-3D image datasets) with unilateral anterior ischemic optic neuropathy (AION).	2D spectral reducing anisotropic diffusion filter	Optimal 3D graph search (graphs are constructed from edge/regional image information and a priori surface smoothness and interaction constraints)	Automated	Average of three experts' tracings as a reference standard was used for evaluation purposes	Overall mean unsigned border positioning error was 6.1 ± 2.9 µm, a result comparable to the interobserver variability (6.9 ± 3.3 µm)	First reported approach for the automated 3D segmentation of intraretinal layers.	Mean segmentation time (after alignment/reg istration) was 4.1 ± 0.9 min (using a Windows XP workstation with a 3.2-GHz Intel Xeon CPU).
Shrinivasan, VJ., 2008, UHR-OCT	Various retinal layers/ segments (6) but main focus on the outer retina segmentation	OCT data from 43 healthy subjects	Median filter (3 pixels) in the transverse direction	Modification of Koozekanani algorithm	Automated	Linear interpolation to correct for segmentation errors	Segmentation accuracy of the outer retinal layers was assessed by comparing automated vs. manually assisted measurements	Quantitative measurements of the outer retinal morphology were used to aid interpretation of the scattering bands posterior to IS/OS juntion visualized on UHR OCT images	Not reported
Ahlers, C., 2008, SDOCT (Cirrus HD-OCT)	Inner and outer borders of the retina along with the volume and area of fPEDs	OCT data from 22 patients with fPED	Morphological filtering to eliminate thin vitreous membranes from the thresholded image	Adaptive thresholding technique and intensity peak detection	Automated	None	Quality control of the automatic segmentation revealed reasonable results in over 90% of examinations	Automatic segmentation facilitated a thickness map showing the configuration of intraretinal fluid in much higher detail. Algorithm is able to track retinal- and subretinal changes in patients with RPE detachments	Not reported

Author, Year, Device	Feature	Data	Preprocessing	Method	Type	Manual	Evaluation Accuracy	Comments	Time
Mayer, M., 2008, SDOCT (Spectralis HRA+OCT, Heidelberg Engineering)	RNFL thickness	OCT data from 5 normal and 7 glaucoma eyes	2D mean filter (kernel size 7x5) for speckle denoising along with complex diffusion filtering to aid segmentation.	Fuzzy C-means clustering technique	Automated	None	97% of the upper and 74% of the lower RNFL layer boundary points lied within a 2 pixel range from the manual segmentation of the evaluation data set	NFL segmentation method of circular OCT scans that is applicable to normal as well as pathological data, different patients and varying scanner settings without parameter adaptation	45 seconds on a 2Ghz Pentium IV for a 512x496 circular B-scan
Bagci, AM., 2008/TDOCT (Stratus OCT) & SDOCT (RTVue 100 OCT, Optovue, Freemont, CA)	Various retinal layers/ segments (6)	Data from healthy subjects: TDOCT (15) and SDOCT (10)	Directional filtering (2D filter with a wedge-shaped pass band)	2D edge detection algorithm based on the first derivative of Gaussian in the vertical direction	Automated	None	Difference between automated and manual segmentation was ≤ 4.2 µm, and almost identical to the difference between manual measurements by three observers (≤4.4 µm)	Edge detection uses: 1) the correlation between adjacent A-scans, 2) gray-level mapping technique to overcome uneven tissue reflectivity and variance across subjects	Not reported
Tolliver, D., 2008, SDOCT (3D OCT Cirrus)	Difficult boundary contours (4)	OCT data from 9 pathological subjects and 2 normative subjects	N/A	Spectral rounding	Automated	For evaluation purposes, manual segmentation was performed for 4 randomly selected scans per subject	The aggregate accuracy range for the detected boundaries was [85-99]%	Algorithm is able to track complex boundary contours in the presence of retinal pathology	Not reported
Farsiu, S., 2008, SDOCT (Bioptigen Inc., Durham, NC)	Drusen area, RPE and RNFL inner border	OCT data from 6 AMD eyes (a total of 228 SDOCT B-scans)	Low-pass filtering	DOCTRAP algorithm based on a modified implementation of the GVF based deformable snake method	Automated /Semi-Automated	Manual correction tool to modify the automated segmentation results. AMD images were also manually segmented by 2 experts for evaluation purposes.	Not reported	Algorithm takes advantage of differences of drusen substructures revealed by SDOCT facilitating drusen area and volume measurements	About 6.5 seconds to automatically segment, display and record drusen locations (image size: 512x1000 pixels) on a Intel Centrino-Duo 2.4 GHz CPU
Gotzinger, E., 2008, PS-OCT	RPE	OCT data from healthy volunteers (1) and patients with AMD (1) and pseudovitellif	Fixed pattern noise removal	Two algorithms: 1) Based on retardation data 2)Based on local variations of the polarization	Automated	None	Not reported	Algorithms facilitated a better visualization and quantification of RPE thickening and RPE atrophies when compared to	Algorithm 1: 8.3 minutes (without preprocessing and cornea compensation) for volumes

				state calculated using Stokes vector analysis				algorithms based on intensity images.	with 60 B-scans (100 A-scans each) Algorithm 2: 31 minutes using an AMD Athlon 64X2 Dual Core Processor 4800+, 2.41 GHz, 2 GB RAM
		orm dystrophy (1)							
Mishra, A., 2009, experimental HR-OCT (high speed)	Various retinal layers	OCT data from healthy and diseased rodent retina	Speckle noise and other typical artifacts in OCT images are handled by using an adaptive vector-valued kernel function in the precise layer boundary optimization step	Modified active contour algorithm by using 1) sparse dynamic programming method and 2) two-step kernel based optimization scheme	Automated	None	Not reported	Algorithm achieves accurate intra-retinal segmentation on retinal OCT images under low image contrast and in the presence of irregularly shaped structural features	5 seconds per image on an Intel Pentium 4 2.4 GHz machine with 1 GB of RAM.
Yazdanpanah, A., 2009, experimental FD-OCT	Various retinal layers (5)	20 OCT images from rodent models (4) of retinal degeneration	None	Modified Chan–Vese's energy-minimizing active contour algorithm (augmented with shape prior and weight terms)	Automated / Semi-Automated (user initialization prior to segmentation)	Manual segmentation for evaluation purposes	An average dice similarity coefficient of 0.85 was obtained when measuring the area similarity between the manual and automated segmentation	First multi-phase framework to segment OCT data that incorporates a circular shape prior based on expert anatomical knowledge of the retinal layers, avoiding the need for training	Not reported
Fabritius, T., 2009, experimental SDOCT	Inner and outer borders of the retina	Data from a healthy volunteer and from patients with ARMD (1) and PCV(1)	No denoising required	Intensity signal-based thresholding segmentation	Automated	Manual segmentation for evaluation purposes	Error smaller than 5 pixels in 99.7 (99.2) % of scans for the RPE (ILM) segmentation	Incorporated 3D intensity information to improve the intensity based segmentation. ILM and RPE can be segmented directly from the OCT data without massive pre-processing in a very faster manner.	About 17-21 seconds for 140 frames with 1022 depth scans

Yi, K., 2009, experimental SDOCT	ONH drusen	OCT data from one exenteration patient and 4 glaucoma patients	Anisotropic diffusion filter	Commercially available software from Amira interfaced with ITK's open source C++ algorithms	Automated	None	Not reported	First segmentation approach that is able to facilitate 3D imaging of the shape, size and location of ONH drusen	Not reported
Abramoff, 2009, SDOCT (Cirrus-OCT)	ONH cup and rim	OCT data (200x200x1024 voxels) from 34 glaucoma patients	None	Multiscale 3-D graph search algorithm to segment three retinal surfaces and a voxel column classification algorithm using a k-NN classifier	Automated	A nine k-NN classifier is used to refine/smooth the appearance of segmentation results. In addition, the correlation between algorithm-determined cup to-disc (c/d) ratio and planimetry-derived c/d by 3 experts was calculated for evaluation purposes	The correlation of algorithm c/d ratio to experts 1, 2, and 3 was 0.90, 0.87, and 0.93, respectively.	First algorithm that shows a high correlation between segmentation results of the ONH cup and rim from SDOCT images and planimetry results obtained by glaucoma experts on the same eye	Not reported
Tumlinson, 2009, experimental FD-OCT	Various retinal layers/segments (8)	OCT data from a dark-adapted human subject	Median filter	Thresholded edge-finding algorithm that first applies directionally biased filtering, finds positive and negative edges using derivative filters, and assigns those edges to layer boundaries based on a set of rules.	Automated	None	None	Algorithm exploited information in adjacent B-scans making simpler the segmentation task used to investigate for the first time depth-resolved slow retinal intrinsic optical signals	Comparable to the calculation of the fast Fourier transform (FFT) for translation of raw spectral data into structural tomograms (volume data: 512x 512x1024 on a Condor computer cluster)
Koprowski, R., 2009, SDOCT (Copernicus)	Retinal contours (inner, outer and others)	Various artificial images and one OCT scan	Median filter	Random Contour detection algorithm based on area analysis	Automated	None	Error analysis only reported for artificial images	Contours extraction depend on parameter selection	Not reported. But authors mentioned computation time is a major drawback of the algorithm

Kajic, V. , 2010, 3DOCT	Various retinal layers (8)	466 B-scans from 17 eyes	Dual-tree complex wavelet (DTCW) denoising	Statistical model based on texture and shape that captures the variance of the training data used to segment unseen data.	Automated	None	Evaluation against a large set of manual segmentations (a difference of only 2.6% against the inter-observer variability)	First time, an error measure is computed from a large manually segmented data set (segmented twice by different operators)	Not reported
Zhihong, H., 2010, SDOCT (Cirrus HD-OCT)	neural canal opening (NCO) and cup at the level of RPE/Bruch□s membrane complex	OCT data from 34 patients (68 eyes) with glaucoma or glaucoma suspicion	None	graph-theoretic approach	Automated	B-spline used to smooth/refine the NCO and cup boundaries. In addition, computer-aided planimetry was performed by 3 experts to create a reference standard	Mean unsigned and signed border differences of 2.81 ± 1.48 pixels (0.084 ± 0.044 mm) and -0.99 ± 2.02 pixels (-0.030 ± 0.061 mm) respectively for NCO segmentation	Algorithm is able to detect natural ONH anatomic structures of and optic cup	Not reported
Chiu, SJ., 2010/SDOCT (Bioptigen Inc., Durham, NC)	Various retinal layers (7)	Data from 10 healthy subjects	Gaussian filter along with rectangular averaging filter (3 × 19 pixels)	Graph-based algorithm and dynamic programming	Automated	Manual segmentation for evaluation purposes	Fully automatic algorithm differed from one of the manual graders by an average of 0.95 pixels.	Automatic initialization that bypasses the need for manual endpoint selection	9.74 seconds per image (on average) for 108 B-scans (64-bit OS, Intel Core2 Duo CPU at 2.53 GHz, and 4 GB RAM).
Lee, K., 2010, SDOCT (Cirrus HDOCT)	ONH cup and rim	27 SDOCT scans (200x200x1024 voxels) from 14 glaucoma patients	Median filtering and averaging Based smoothing	Multiscale 3-D graph search algorithm to segment four retinal surfaces and a	Automated	Local fitting method using the convex hulls of the segmentation to refine/smooth the contours of the ONH rim and cup. In addition, two glaucoma experts annotated the cup and rim area in stero- color photographs using planimetry to create the reference standard for evaluation	Unsigned error for the optic disc cup was 2.52+/-0.87 pixels (0.076+/-0.026 mm) and for the neuroretinal rim was 2.04+/-0.86 pixels (0.061+/-0.026 mm).	Fast and fully automatic method to segment the optic disc cup and rim in 3-D SD-OCT volumes	About 132 S (80 seconds to segment 4 intraretinal surfaces using the multiscale 3-D graph search approach, and 52 seconds for the feature extraction and classification) on a PC (Microsoft Windows XP Professional x64 edition,

Table 1. Overview of OCT segmentation approaches.

									purposes		Intel Core 2 Duo CPU at 3.00 GHz, 4GB RAM)
Lu, S., 02010, SDOCT (Spectralis OCT, Heidelberg Engineering)	Various retinal layers (5)	OCT data from 4 normal healthy eyes	Bilateral filter and median filter	Algorithm based on the Canny's edge detector for the non-vessel sections. Linear interpolation is used for the layer boundaries in the vessel sections	Automated	Manual segmentation for evaluation purposes (16 OCT images)	Segmentation errors for the RNFL were less than 5 µm on average	Algorithm first detects the retinal blood vessels and then split the OCT image into multiple vessel and non-vessel sections.	Not reported
Yang, Q., 2010, SDOCT (Topcon 3D OCT-1000)	Various retinal layers (9)	OCT data (38 Scans) from 38 individuals, 19 glaucoma patients and 19 controls	None	Algorithm based on a dual-scale gradient information and a shortest path Search using dynamic programming	Automated	Manual segmentation for evaluation purposes	Overall the ICC of each boundary was above 0.94, the mean coefficient of variation was less than 7.4%, and the mean standard deviation was less than 2.8µm.	Algorithm is able to segment low-intensity and low-contrast OCT images in a very short time without degrading the accuracy In addition, pre-extraction of vessel locations, which is not a trivial operation, is unnecessary	About 45 seconds for each 3D volume (480x512x128 voxels) in normal segmentation processing mode and 16 seconds in fast segmentation mode using A-scan reduction technique
Quellec, G., 2010, SDOCT (Cirrus, HD-OCT)	Various retinal layers (10) along with fluid-filled regions	OCT data from 13 normal eyes and from 23 eyes with CNV, intra-, and sub-retinal fluid and pigment epithelial detachment	Wavelets	Multiscale 3-D graph search approach	Automated	Manual segmentation for evaluation purposes	Mean unsigned surface positioning errors were less than 6 µm.	Confirmed that useful 3-D textural information can be also extracted from SD-OCT scans to aid local retinal abnormality detection.	70 seconds per eye for 10 layer detection on a 200x1024x200 voxel volume using a standard PC at 2.4 GHz; (800 MB of RAM)

8. References

Abràmoff, MD., Lee, K., Niemeijer, Wallace, L., Alward, M., Greenlee, EC., Garvin, MK., Sonka, M. & Kwon, YH. (2009). Automated Segmentation of the Cup and Rim from Spectral Domain OCT of the Optic Nerve Head. *Invest. Ophthalmol. Vis. Sci.* 2009 50: 5778-5784

Ahlers, C., Simader, C., Geitzenauer, W., Stock, G., Stetson, P., Dastmalchi, S & Schmidt-Erfurth, U. (2008). Automatic segmentation in three-dimensional analysis of fibrovascular pigmentepithelial detachment using high-definition optical coherence tomography. *Br. J Ophthalmol.* 92, 197-203

Aguirre AD., Hsiung, P., Ko, P., Hartl, TH.& Fujomoto JG. (2003) High-resolution optical coherence microscopy for high-speed in vivo cellular imaging. *Optics Lett.* 2064-2066 28

Alirezaie, J., Jernigan, M E., Nahmias, C., (1997). Neural Network-Based Segmentation of Magnetic Resonance Images of the Brain, *IEEE Trans. on Nuclear Science*, 44:194-8

Andreasen, NC., Rajarethinam, J., Cizadlo, T. Arndt, S., Swayze, VW., Flashman, LA., O'Leary. DS, Ehrhardt, JC. & Yuh, WT. (1996) Automatic atlas-based volume estimation of human brain regions from MR images. *J Comp. Assist. Tom.*, 20:98–106

Bagci, AM., Shahidi, M., Ansari, R., Blair, M., Blair, NP & Zelkha, R. (2008). Thickness profiles of retinal layers by optical coherence tomography image segmentation. *Amer. J Ophthalmol.*, vol. 146, no. 5, pp. 679–687

Baroni, M., Fortunato, P. & Torre, AL. (2007). Towards quantitative analysis of retinal features in optical coherence tomography. *Medical Engineering and Physics* 29(4), 432–441

Bizheva, K., Pflug, R., Hermann, B., Povazay, B., Sattmann, H., Qiu, P., Anger, E., Reitsamer, H., Popov, S., Taylor, JR., Unterhuber, A., Ahnelt, P. & Drexler, W. (2006). Optophysiology: depth-resolved probing of retinal physiology with functional ultrahigh-resolution optical coherence tomography. *Proc. Natl. Acad. Sci. USA* 28, 103, 5066-71

Boppart, SA., Drexler, W., Morgner, U., Kirtner, FX. & Fujimoto, JG. (1999). Ultrahigh Resolution and Spectroscopic OCT Imaging of Cellular Morphology and Function, *Proceedings of Inter-Institute Workshop on In Vivo Optical Imaging at the National Institutes of Health,* A. H. Gandjbakhche, Ed., pp. 56–61

Boykov, Y., & Funka-Lea, G. (2006). Graph cuts and efficient N-D image segmentation. *Int. J Comput. Vision,* vol. 70, pp. 109–131

Boyer, KL., Herzog, A., Roberts, C. (2006). Automatic recovery of the optic nervehead geometry in optical coherence tomography. *IEEE Trans Med Imaging.* May; 25(5):553-70. PubMed PMID: 16689260.

Brezinski, ME., Tearney, GJ., Bouma, BE., Izatt, JA., Hee, MR., Swanson, EA., Southern, JF., & Fujimoto, JG. (1996). Optical coherence tomography for optical biopsy: properties and demonstration of vascular pathology. *Circulation, 93 (6)*: pp. 1206-1213.

Cabrera Fernández, D., Villate, N., Puliafito, CA. & Rosenfeld, PJ. (2004). Comparing total macular volume changes measured by Optical Coherence Tomography with retinal lesion volume estimated by active contours. *Invest. Ophthalmol. Vis. Sci.* 45: E-Abstract 3072.

Cabrera Fernández, D. (2005a). Delineating fluid-filled region boundaries in optical coherence tomography images of the retina," *IEEE Trans. Med. Imag.*,vol. 24, no. 8, pp. 929–945

Cabrera Fernández, D. Salinas, HM & Puliafito, CA. (2005b). Automated detection of retinal layer structures on optical coherence tomography images. *Optics Express* 13(25), 10,200–10,216

Cabrera Fernández, Somfai, GM., Tátrai, E., Ranganathan, S., Yee, DC., Ferencz, M. & Smiddy, WE. (2008) Potentiality of Intraretinal Layer Segmentation to Locally Detect Early Retinal Changes in Patients With Diabetes Mellitus Using Optical Coherence Tomography *Invest. Ophthalmol. Vis. Sci.* 49: E-Abstract 2751.

Cabrera DeBuc, D. & Somfai, GM. (2010). Early detection of retinal thickness changes in diabetes using Optical Coherence Tomography," Med. Sci. Monit. 16(3), MT15–MT21

Cense, B., Chen, TC., Hyle, P.B, Pierce,MC &de Boer, JF. (2002). In vivo depth-resolved birefringence measurements of the human RNFL by PS-OCT. *Optics Lett.* 27, 1610-1612

Cense, B., Nassif, N., Chen, T., Pierce, M., Yun, SH., Park, B., Bouma, B., Tearney, B. & de Boer, JF (2004). Ultrahigh resolutionhigh-speed retinal imaging using spectral-domain optical coherence tomography, *Opt. Express.* 12(11), 2435–2447 (2004).

Chen, Z., Milner, TE., Dave, D. & Nelson JS. (1997). Optical Doppler tomographic imaging of fluid flow velocity in highly scattering media. Optics Lett. 22, 64-66

Cheng, K S., Lin, J S. & Mao, CW. (1996). The Application of Competitive Hopfield Neural Network to Medical Image Segmentation. *IEEE Trans. on Med. Img.*, 15:560-7

Chiu, SJ.,Li, CT., Nicholas, P.,Toth, CA., Izatt, JA, & Sina Farsiu. (2010). Automatic segmentation of seven retinal layers in SDOCT images congruent with expert manual segmentation. *Optic Express.* Vol. 18, No. 18. pp. 19413-19428

Choma, MA., Sarunic, MV., Yang, C., Izatt, JA. (2003). Sensitivity advantage of swept source and Fourier domain optical coherence tomography. *Optics Express.* 11: 2183-2189

Cootes, T F., Edwards, G J., Taylor, C J. (2001). Active Appearance Models. *IEEE Trans. Pattern Analysis and Machine Intelligence*, 23: 681-85

deBoer, JF., Milner, TE., vanGemert, MJC. & Nelson, JS. (1997). Two-dimensional birefringence imaging in biological tissue by polarization-sensitive optical coherence tomography. *Optics Letters*, *22*(12), 934-936

deBoer, JF., Shrinivas, SM., Malekafzali, A., Chen, Z. & Nelson, JS. (1998). Imaging thermally damaged tissue by polarization sensitive OCT. *Optics Express.* 3, 212-218

de Boer, JF., Cense, B., Park, BH., Pierce, MC., Tearney, GJ., & Bouma, BE. (2003). Improved signal-to-noise ratio in spectral-domain compared with time-domain optical coherence tomography. *Optics Letters*, *28* (21), 2067-2069

Ding, Z., Zhao, Y.,Ren, H., Nelson, JS. & Chen, Z. (2002). real-time phase-resolved OCT and optical Doppler tomography. Optic Express. 10, 236-245

Drexler, W. & Fujimoto, JG. (2008). State-of-the-art retinal optical coherence tomography, *Prog. Retin. Eye Res.* 27(1), 45–88

Fabritius, T., Makita, S., Miura, M., Myllyla, R. & Yasuno, Y. (2009). Automated segmentation of the macula by optical coherence tomography. *Opt. Express* 17(18), 15659-15669

Farsiu, S., Chiu, SJ., Izatt, JA., Toth, CA. (2008). Fast detection and segmentation of drusen in retinal optical coherence tomography images. *Photonics West, Ophthalmic Technologies.* San Jose, CA; 68440D-68441-68412

Fercher, AF., Hitzenberger, CK., Kamp, G. & Elzaizt, SY. (1995). Measurement of intraocular distances by backscattering spectral interferometry. *Opt. Commun.* 117(1-2), 43–48

Fercher, AF., Drexler, W., Hitzenberger, C.K. (2003). Optical coherence tomography. Principles and applications. *Rep Prog Phys.* 66: 239-303

Ford, L. & Fulkerson, D. (1956). Maximal flow through a network. *Canadian Journal of Mathematics.* 8. 399-404

Fuller, AR., Zawadzki, RJ., Choi, S., Wiley, DF., Werner, JS. & Hamann, B. (2007). Segmentation of Threedimensional Retinal Image Data. *IEEE Transactions on Visualization and Computer Graphics* 13(6), 1719–1726

Fujimoto, JG. (2003). Optical coherence tomography for ultrahigh resolution in vivo imaging. *Nature Biotechnology*, Vol. 21, No. 11, pp 1361-67

Garvin, MK., Abramoff, MD., Kardon, R., Russell, SR., Wu, X. & Sonka, S. (2008). Intraretinal Layer Segmentation of Macular Optical Coherence Tomography Images Using Optimal 3-D Graph Search. *IEEE Transactions on Medical Imaging* 27(10), 1495 – 1505

George, A., Dillenseger, JA., Weber, A. & Pechereau, A. (2000). Optical coherence tomography image processing. *Investigat. Ophthalmol. Vis.Sci.*, vol. 41, pp. S173–S173

Gonzalez, RC. & Woods, RE. (1992) *Digital Image Processing.* Addison-Wesley

Götzinger, E., Pircher, M., Geitzenauer, W., Ahlers, C., Baumann, B., Michels, S., Schmidt-Erfurth, U. & Hitzenberger, CK. (2008). Retinal pigment epithelium segmentation by polarization sensitive optical coherence tomography. Opt. Express 16(21), 16410–16422

Greig, D., Porteous, B. & Seheult, A. (1989). Exact maximum a posteriori estimation for binary images. *Journal of the Royal Statistical Society* 51(2) (1989) 271-279

Gregori, G. & Knighton, RW. (2004). A Robust Algorithm for Retinal Thickness Measurements using Optical Coherence Tomography (Stratus OCT). *Invest. Ophthalmol.Vis.Sci.*45:E-Abstract-3007

Gregori, G., Knighton, RW., Jiao, S., Huang, X., Rosenfeld, PJ. & Puliafito, CA. 3–D OCT Maps of Retinal Pathologies. (2005) *Invest. Ophthalmol. Vis. Sci.* 2005 46: E-Abstract 1055.

Gregori, G., Gregori, NZ., Knighton, RW., Lujan, BJ. Puliafito, CA. & Rosenfeld, PJ. (2008). Imaging Drusen With Spectral Domain Optical Coherence Tomography. *Invest. Ophthalmol.Vis.Sci.*49:E-Abstract-4234
Greig, D., Porteous, B., Seheult, A. (1989). Exact maximum a posteriori estimation for binary images. *Journal of the Royal Statistical Society.* 51(2), 271-279

Haeker, M., Abràmoff, M., Kardon, R., Sonka, M. (2006). Segmentation of the surfaces of the retinal layer from OCT images. *Med Image Comput Comput Assist Interv.* 9 (Pt 1):800-7. PubMed PMID: 17354964.

Haralick, RM. & Shapiro, LG. (1985). Image segmentation techniques. *Comput. Vis. Graph. Im. Proc.*, 29:100–132

Hausler, G. & Lindner, MW. (1998). Coherence Radar and Spectral Radar. New tools for dermatological diagnosis. *J Biomed Opt* 1998; 3: 21-31

Hee, MR., Izatt, JA., Swanson, EA., Huang, D., Schuman, JS., Lin, CP., Puliafito, CA. & Fujimoto, JG. (1995a). Optical coherence tomography of the human retina. *Arch. Ophthalmol.* 113, 325-32

Hee, MR., Izatt, JA., Swanson EA., Huang, D., Schuman, JS., Puliafito, CA. & J. G. Fujimoto. (1995b). Optical coherence tomography for micron-resolution ophthalmic imaging. *IEEE Eng. Med. Biol.*, vol. 14, pp. 67–76

Hee, MR. (1997). Optical Coherence Tomography of the eye. Thesis (PhD). Massachusetts Institute of Technology, Source DAI-B 58/04, p. 1952.

Held, K., Kops, ER., Krause, BJ., Wells, WM. Kikinis, R., & Muller-Gartner, HW. (1997). Markov random field segmentation of brain MRI images. *IEEE T. Med. Imag.*, 16(6)

Hermann JM., Pitris, C., Bouma, BE., Boppart, SA., Jesser, CA., Stamper, DL., Fujimoto, JG., Brezinski, ME. (1999). High-resolution imaging of normal and osteoarthritic cartilage with OCT. J. Rheumatol. 26, 627-635

Hermann, B., Fernandez, EJ., Unterhubner, A. Sattmann,H., Fercher, AF., Drexler, Prieto, WPM., & Artal, P. (2004). Adaptive-optics ultrahigh-resolution optical coherence tomography. *Opt. Lett.* 29, 2142-2144

Hermann, B., Považay, B., Unterhuber, A. Lessel, M., Sattmann, H., Schmidt-Erfurth, U. & Drexler, W. (2006). Optophysiology of the Human RetinaWith Functional Ultrahigh Resolution Optical Coherence Tomography. Invest. Ophthalmol. Vis. Sci. 2006 47: E-Abstract 1672

Herzog, A., Boyer, KL. & Roberts, C. (2004). Robust Extraction of the Optic Nerve Head in Optical Coherence Tomography. *CVAMIA-MMBIA*, LNCS 3117, pp. 395–407

Hu, Z., Abramoff, MD., Kwon, YH., Lee, K., Garvin, M. (2010). Automated Segmentation of Neural Canal Opening and Optic Cup in 3-D Spectral Optical Coherence Tomography Volumes of the Optic Nerve Head. *Invest Ophthalmol Vis Sci.* Jun 16. [Epub ahead of print] PubMed PMID: 20554616

Huang, D., Swanson, EA., Lin, CP., Schuman, JS., Stinson, GW., Chang, W., Hee, MR., Flotte,T., Gregory, K., Puliafito, CA. & Fujimoto JG. (1991). Optical coherence tomography. *Science* 254, 1178–81

Huang, Y., Cideciyan, AV., Papastergiou, GI., Banin, E., Semple-Rowland, SL., Milam, AH., Jacobson, SG. (1998). Relation of optical coherence tomography to microanatomy in normal and rd chickens. *Invest. Ophthalmol. Vis. Sci.* 39: 2405-2416.

Ishikawa, H., Piette, S., Liebmann, JM. & Ritch, R. Detecting the inner and outer borders of the retinal nerve fiber layer using optical coherence tomography. (2002). *Graefe's Archive for Clinical and Experimental Ophthalmology*. May;240(5):362-71

Ishikawa, I., Stein, DM., Wollstein, G., Beaton, S., Fujimoto, JG. & Schuman, JS. (2005). Macular Segmentation with Optical Coherence Tomography. *Investigative Ophthalmology and Visual Science (IOVS)* 46(6), 2012–2017

Izatt, JA., Hee, MR., Swanson, EA., Lin,CP., Huang, D., Schuman, JS., Puliafito, CA. & Fujimoto, JG. (1994a). Micrometer-scale resolution imaging of the anterior eye in vivo with optical coherence tomography. *Arch. Ophthalmol.* 112, 1584-9

Izatt, JA., Hee, MR., Owen, GM.,Swanson, EA. & Fujimoto, JG. (1994b). Optical coherence microscopy in scattering media. *Optics Lett.* 19. 590-592

Izatt, JA., Kulkami, MD., Wang, H-W., Kobayashi, K., & Sivak MV. (1996). Optical coherence tomography and microscopy in gastrointestinal tissues. *IEEE J Selected Topics Quantum Electron.* 2, 1017-1028

Izatt, JA., Kulkami, MD.,Yazdanfar, S., Barto, JK. & Welch, AJ. (1997). In vivo bidirectional color Doppler flow imaging of picoliter blood volumes using OCT. *Optics Lett.* 22, 1439-1441

Kajić, V., Považay, B., Hermann, B., Hofer, B., Marshall, D., Rosin, PL. & Drexler, (2010). W. Robust segmentation of intraretinal layers in the normal human fovea using a novel statistical model based on texture and shape analysis. *Opt. Express* 18(14), 14730–14744

Kocaoglu, OP., Uhlhorn, SR., Hernandez, E., Juarez, RA., Will, R Parel, J-M., & Manns, F. (2007). Simultaneous Fundus Imaging and Optical Coherence Tomography of the Mouse Retina.*Invest. Ophthalmol. Vis. Sci.* 48: 1283-1289.

Kolmogorov, V. & Zabih, R. (2004). What energy functions can be minimized via graph cuts?, *IEEE PAMI*, vol. 26, pp. 147–159

Koozekanani, D., Boyer, KL.,Roberts, C. (2001). Retinal Thickness Measurements in Optical Coherence Tomography Using a Markov Boundary Model. *Medical Imaging, IEEE Transactions on* 20(9), 900–916

Koprowski, R. & Wrobel, Z. (2009). Layers recognition in tomographic eye image based on random contour analysis. *Computer recognition Syst. 3, AISC 57*, Kurzynski, M. & Wozniak, M. (Eds), pp. 471-478, Springer-Verlag, Berlin Heidelberg

Lancaster, JL., Rainey, LH., Summerlin, JL., Freitas, CS., Fox, PT., Evans, AC., & Mazziotta, JC. (1997). Automated labeling of the human brain: A preliminary report on the development and evaluation of a forward-transform method. Human Brain Mapping., 5:238-242

Lee, K., Abramoff, MD., Niemeijer, M., Garvin, MK., Sonka, M. (2010). 3-D segmentation of retinal blood vessels in spectral-domain OCT volumes of the optic nerve head. *Proc. of SPIE Medical Imaging: Biomedical Applications in Molecular, Structural, and Functional Imaging*, vol. 7626, p. 76260V, 2010

Leitgeb, RA., Schmetterer, I., Drexler, W., Fercher, AF., Zawadzki, RJ. & Bajraszewskit, J. (2003). Real-time assessment of retinal blood flow with ultrafast acquisition by color Doppler Fourier domain optical coherence tomography. *Optics Express*; 11: 3116-3121

Li, SZ. (1995) *Markov random field modeling in computer vision.* Springer-Verlag, ISBN:4-431-70145-1, London, UK

Liu,Y., Chen, M., Ishikawa, H., Wollstein, G., Schuman, JS. & Rehg, JM. (2010). In: *Automated Macular Pathology Diagnosis in Retinal OCT Images Using Multi-Scale Spatial Pyramid with Local Binary Patterns.*T. Jiang et al. (Eds.), pp. 1–9, MICCAI 2010, Part I, LNCS 6361, Springer-Verlag, Berlin, Heidelberg

Lu, S., Cheung, C., Liu, J., Lim, S., Leung, C. & Wong, T. (2010). Automated Layer Segmentation of Optical Coherence Tomography Images. *IEEE Trans Biomed Eng.*; 57(10), 2605-8

Maintz, JBA. & Viergever., MA. (1998). A survey of medical image registration. *Med. Im. Anal.*, 2:1–36

Mayer, MA., Tornow, RP., Bock, R., Hornegger, J. & Kruse, FE. (2008). Automatic Nerve Fiber Layer Segmentation and Geometry Correction on Spectral Domain OCT Images Using Fuzzy C-Means Clustering. *Invest. Ophthalmol. Vis. Sci.* 49: E-Abstract 1880

Michelson AA. & Morley EW. (1887). Philos. Mag. S.5, 24 (151), 449-463

Mishra, A., Wong, A., Bizheva, K. & Clausi, DA. (2009). Intra-retinal layer segmentation in optical coherence tomography images. *Opt. Express* 17(26), 23719–23728

Mitsui, T. (1999). Dynamic range of optical reflectometry with spectral interferometry. *Jap J Appl Phys* (Part 1 Regular Papers Short Notes & Review Papers); 38: 6133-6137

Mohamed, NA., Ahmed, MN., Farag A. (1998). Modified Fuzzy C-mean in Medical Image Segmentation. *Proceedings of the 20th Annual International Conference of the IEEE,* 3:1377-80.

Morgner, U., Drexler, W., Kartner, FX., Li, XD., Pitris, C., Ippen, EP., Fujimoto, JG. (2000). Spectroscopic optical coherence tomography. *Optics Lett.* 25, 111-113

Mujat, M., Chan, R., Cense, B., Park, B., Joo, C., Akkin, T., Chen, T. & de Boer, J. (2005). Retinal nerve fiber layer thickness map determined from optical coherence tomography images. *Optics Express* 13(23). 9480–9491

Novotny, HR & Alvis, DL. (1961). A method of photographing fluorescence in circulating blood in the human retina. *Circulation.* 24(1):82–86

Osher, S. & Sethian, J. (1988). Fronts Propagating with curvature-dependent speed: algorithms based on Hamilton-Jacobi formulations. *J Comp. Phys.*, 79: 12-49

Pal, NR. & Pal., SK. (1993). A review on image segmentation techniques. *Patt. Rec.*, 26:1277–1294

Pappas, TN. (1992). An adaptive clustering algorithm for image segmentation. *IEEE Trans. Signal Processing.* 40(4):901-914

Pathak, SD., Grimm, PD., Chalana, V. & Kim, Y. (1998). Pubic arch detection in transrectal ultrasound guided prostate cancer therapy. *IEEE T. Med. Imag.*, 17:762–771

Podoleanu, AG., Dobre, GM., Cucu, RG., Rosen, R., Garcia, P., Nieto, J., Will, D., Gentile, R., Muldoon, T., Walsh, J., Yannuzzi, L.A., Fisher, Y., Orlock, D., Weitz, R., Rogers, J.A., Dunne, S., Boxer, A. (2004). Combined multiplanar optical coherence tomography and confocal scanning ophthalmoscopy. *J Biomed. Opt. 9, 86–93*

Puliafito CA. (1996). *Optical Coherence Tomography of Ocular Diseases.* Thorofare, NJ: SLACK Inc

Quellec, G., Lee, K., Dolejsi, M., Garvin, MK., Abràmoff, MD. & Sonka, M. (2010). Three-dimensional analysis of retinal layer texture: identification of fluid-filled regions in SD-OCT of the macula. *IEEE Trans. Med. Imaging* 29(6), 1321–1330

Rajapakse, C., Giedd, JN. & Rapoport, JL. (1997). Statistical approach to segmentation of single-channel cerebral mr images. *IEEE T.Med. Imag.*, 16:176-186

Ren, H. (2002). Phase-resolved functional Optical Coherence Tomography: simultaneous imaging of in situ tissue structure, blood flow velocity, standard deviation, birefringence, and Stokes vectors in human skin. *Optics Lett.* 27, 1702-1704

Ruggeri, M., Wehbe, H., Jiao, S., Gregori, G., Jockovich, ME., Hackam, A., Duan, Y. & Puliafito, CA. (2007) In Vivo Three-Dimensional High-Resolution Imaging of Rodent Retina with Spectral-Domain Optical Coherence Tomography. *Invest. Ophthalmol. Vis. Sci.* 48: 1808-1814

Sahoo, PK., Soltani, S.,Wong, AKC. (1988). A survey of thresholding techniques. *Comput Vision Graphics Image Process* 41:233–260

Sarkar, S., Boyer, K. (1991). Optimal impulse response zero crossing based edge detectors. *Computer Vision Graphics Image Process: Image Understanding* 54, 224–243

Shahidi, M., Wang, Z. & Zelkha, R. (2005). Quantitative Thickness Measurement of Retinal Layers Imaged by Optical Coherence Tomography. *American Journal of Ophthalmology* 139(6), 1056 – 1061

Smith RT, Chan JK, Nagasaki T, Sparrow JR, Barbazetto I. (2005). Automated detection of macular drusen using geometric background leveling and threshold selection. *Arch Ophthalmol* 2005;123:200-206

Sylwestrzak, M., Szkulmowski, M., Szlag, D. & Targowski, P. (2010). Real-time imaging for SDOCT with massively parallel data processing. *Photonics Letter of Poland.* vol. 2(3), 137-139.

Sziranyi, T., Zerubia, J., Czuni, L., Geldreich, D. & Kato, Z. (2000). Image Segmentation Using Markov Random Field Model in Fully Parallel Cellular Network Architectures. *Real-Time Imaging.* 6, 195-211

Szulmowski, M., Wojtkowski, M., Sikorski, B., Bajraszewski, B., Srinivasan, VJ., Szkulmowska, A., Kaluzny, JJ., Fujimoto, JG & Kowalczyk, A. (2007). Analysis of posterior retinal layers in spectral optical coherence tomography images of the normal retina and retinal pathologies. *Journal of Biomedical Optics* 12(4)

Talairach, J. & Tournoux, P. (1988). *Co-Planar Stereotaxic Atlas of the Human Brain. 3-Dimensional Proportional System: An Approach to cerebral Imaging.* Thieme Medical Publisher, Inc., Stuttgart, NY

Tan, O., Li,. G., Lu, AT., Varma, R., Huang, D. (2008). Advanced Imaging for Glaucoma Study Group. Mapping of macular substructures with optical coherence tomography for glaucoma diagnosis. *Ophthalmology.* Jun;115(6):949-56

Tolliver, DA., Koutis, Y., Ishikawa, H., Schuman, JS., & Miller, GL. (2008). Automatic Multiple Retinal Layer Segmentation in Spectral Domain OCT Scans via Spectral Rounding. *Invest. Ophthalmol. Vis. Sci.* 49: E-Abstract 1878

von der Malsburg, C. (1981). The correlation theory of brain function. *Technical report.* Max-Planck-Institute Biophysical Chemestry

von Helmholtz, H. (1851) In World Encyclopedia. Oxford University Press, 2005.

Wang, DL. & Terman. D. (1995). Locally excitatory globally inhibitory oscillator networks. *IEEE Transactions on Neural Networks.* 6(1):283-286

Wang, DL. & Terman, D. (1997). Image segmentation based on oscillatory correlation. Neural Computing.9:805-836.

Wang, S., Zhu, W Y., Liang, Z P. (2001). ShapeDeformation: SVM Regression and Application to Medical Image Segmentation. *Eight International Conference on Computer Vision*, 2:209-16

Westphal, V., Yazdanfar, S, Rollins, AM., Izatt, JA. (2002) Real time, high-velocity resolution color Doppler Optical Coherence Tomography. *Optics Lett.* 27, 34-36

Wojtkowski M., Bajraszewski T., Targowski P., Kowalczyk A. (2003). Real-time in vivo imaging by high-speed spectral optical coherence tomography. *Opt Lett.* 2003 Oct 1;28(19):1745-7

Wong, RC. (2002). Visualization of subsurface blood vessels by color Doppler Optical Coherence Tomography in rats: before and after hemostatic therapy. *Gastrointest. Endosc.* 55, 88-95

Yang, Q., Reisman, CA., Wang, z., Fukuma, Y., Hangai, m., Yoshimura, N., Tomidokoro, A., Araie, M., Raza, AR., Hood, DC. & Chan, K. (2010). Automated layer segmentation

of macular OCT images using dual-scale gradient information. *Optics Express*. Vol. 18, No. 20, pp. 21294-21307

Yazdanfar, S., Rollins, AM., Izatt, JA. (2003). In vivo imaging of human retinal flow dynamics by color Doppler Optical Coherence Tomography. *Arch. Ophthalmol*. 121, 235-239

Yazdanpanah, A., Hamarneh, G., Smith, B., Sarunic, M. (2009). Intra-retinal layer segmentation in optical coherence tomography using an active contour approach. *Med Image Comput Comput Assist Interv*. 12(Pt 2):649-56

Yezzi ,A., Tsai, A., Willsky, A. (1999). A statistical approach to snakes for bimodal and trimodal imagery. *Proceedings of the seventh IEEE international conference on computer vision*, pp. 898–903.Washington, DC: IEEE Computer Society

Yi, K., Mujat, M., Park, BH., Sun, W., Miller, JW., Seddon, JM., Young, LH., de Boer, JF. & Chen, TC. (2009). Spectral domain optical coherence tomography degeneration for quantitative evaluation of drusen and associated structural changes in non-neovascular age-related macular. *Br JOphthalmol*. 93: 176-181

Zawadzki, RJ., Jones, SM., Olivier, SS., Zhao, M., Bower, BA., Izatt, JA., Choi, S., Laut, S. & Werner, JS. (2005). Adaptive-optics optical coherence tomography for high-resolution and high-speed 3D retinal in vivo imaging. Optics Express. Vol. 13, No. 21, pp. 8533-8546

Zhao, Y. (2000) Phase-resolved Optical Coherence Tomography and Optical Doppel Tomography for imaging blood flow in human skin with fast scanning speed and high velocity sensitivity. *Optics Lett*. 25, 114-116
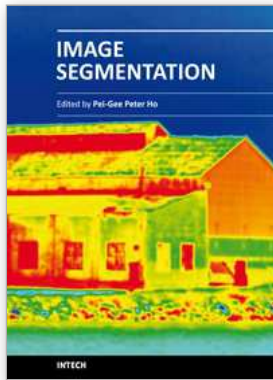
Image Segmentation

Edited by Dr. Pei-Gee Ho

It was estimated that 80% of the information received by human is visual. Image processing is evolving fast and continually. During the past 10 years, there has been a significant research increase in image segmentation. To study a specific object in an image, its boundary can be highlighted by an image segmentation procedure. The objective of the image segmentation is to simplify the representation of pictures into meaningful information by partitioning into image regions. Image segmentation is a technique to locate certain objects or boundaries within an image. There are many algorithms and techniques have been developed to solve image segmentation problems, the research topics in this book such as level set, active contour, AR time series image modeling, Support Vector Machines, Pixon based image segmentations, region similarity metric based technique, statistical ANN and JSEG algorithm were written in details. This book brings together many different aspects of the current research on several fields associated to digital image segmentation. Four parts allowed gathering the 27 chapters around the following topics: Survey of Image Segmentation Algorithms, Image Segmentation methods, Image Segmentation Applications and Hardware Implementation. The readers will find the contents in this book enjoyable and get many helpful ideas and overviews on their own study.

How to reference

In order to correctly reference this scholarly work, feel free to copy and paste the following:

Delia Cabrera DeBuc (2011). A Review of Algorithms for Segmentation of Retinal Image Data Using Optical Coherence Tomography, Image Segmentation, Dr. Pei-Gee Ho (Ed.), ISBN: 978-953-307-228-9, InTech, Available from: http://www.intechopen.com/books/image-segmentation/a-review-of-algorithms-for-segmentation-of-retinal-image-data-using-optical-coherence-tomography

INTECH
open science | open minds